JOURNAL OF PETROLOGY | VOLUME 51 | NUMBER 11 | PAGES 2277–2301 | 2010 | doi:10.1093/petrology/egq057

The Annandagstoppane Granite, East Antarctica: Evidence for Archaean Intracrustal Recycling in the Kaapvaal–Grunehogna Craton from Zircon O and Hf Isotopes

HORST R. MARSCHALL[1]*, CHRIS J. HAWKESWORTH[2], CRAIG D. STOREY[3], BRUNO DHUIME[1], PHILIP T. LEAT[4], HANS-PETER MEYER[5] AND SUNE TAMM-BUCKLE[4,†]

[1]DEPARTMENT OF EARTH SCIENCES, UNIVERSITY OF BRISTOL, WILLS MEMORIAL BUILDING, QUEEN'S ROAD, BRISTOL BS8 1RJ, UK

[2]UNIVERSITY OF ST. ANDREWS, COLLEGE GATE, NORTH STREET, ST. ANDREWS KY16 9AJ, UK

[3]SCHOOL OF EARTH AND ENVIRONMENTAL SCIENCES, UNIVERSITY OF PORTSMOUTH, BURNABY BUILDING, BURNABY ROAD, PORTSMOUTH PO1 3QL, UK

[4]BRITISH ANTARCTIC SURVEY, MADINGLEY ROAD, HIGH CROSS, CAMBRIDGE CB3 0ET, UK

[5]INSTITUT FÜR GEOWISSENSCHAFTEN, UNIVERSITÄT HEIDELBERG, IM NEUENHEIMER FELD 234–236, 69120 HEIDELBERG, GERMANY

RECEIVED APRIL 23, 2010; ACCEPTED SEPTEMBER 6, 2010

The Grunehogna Craton (GC, East Antarctica) is interpreted as part of the Archaean Kaapvaal Craton of southern Africa prior to Gondwana breakup. The basement of the GC is exposed only within a small area comprising the dominantly leucocratic Annandagstoppane (ADT) S-type granite. The granite (and hence the craton) has been dated previously only by Rb–Sr and Pb–Pb mica and whole-rock methods. Here, the crystallization age of the granite is determined to be 3067 ± 8 Ma by U–Pb dating of zircon. This age is coeval with that of granitoids and volcanic rocks in the Swaziland and Witwatersrand blocks of the Kaapvaal Craton. Inherited grains in the ADT granite have ages of up to 3433 ± 7 Ma, and are the first evidence of Palaeoarchaean basement in Dronning Maud Land. The age spectrum of the inherited grains reflects well-known tectono-magmatic events in the Kaapvaal Craton and forms important evidence for the connection of the GC to the Kaapvaal Craton for at least 2·5 billion years and probably longer. Whole-rock chemistry and zircon O isotopes demonstrate a supracrustal sedimentary source for the granite, and Hf model ages show that at least two or three crustal sources contributed to the magma with model ages of ~3·50, ~3·75 and possibly ~3·90 Ga. The 3·1 Ga granites covering ~60% of the outcrop area of the Kaapvaal–Grunehogna Craton played a major role in the mechanical stabilization of the continental crust during the establishment of the craton in the Mesoarchaean. Combined zircon Hf–O isotope data and the lack of juvenile additions to the crust in the Mesoarchaean strongly suggest that crustal melting and granite formation was caused by the deep burial of clastic sediments and subsequent incubational heating of the crust. Intracrustal recycling of this type may be an important process during cratonization and the long-term stabilization of continental crust.

KEY WORDS: *Hf model age; zircon O isotopes; Dronning Maud Land; Archaean; craton*

*Corresponding author. Telephone: +44-117-3315006. Fax: +44-117-9253385. E-mail: Horst.Marschall@bristol.ac.uk
†Present address: Glenridge, Weare Giffard, Bideford EX39 4QN, UK.

INTRODUCTION

Investigations of the early Archaean and Hadean rock and mineral record in increasing detail have established the onset of continental crust formation on Earth as early as 4·4 Ga, shortly after planetary accretion (Wilde *et al.*, 2001). By the end of the Archaean at 2·5 Ga, an estimated 30–80% of today's volume of continental crust had formed (e.g. Collerson & Kamber, 1999; Taylor & McLennan, 2009). However, it remains unclear what the rate and dominant mechanisms of formation were throughout the Hadean and Archaean, and when the fragments of buoyant, differentiated crust were large and stable enough to form the first cratons; that is, the nuclei of the modern continents. Cratons are characterized by a lack of penetrative internal deformation and the lack of significant vertical movement over time scales of hundreds of millions to billions of years. The stabilization of cratons was achieved by intracrustal differentiation by tectonic, metamorphic and magmatic processes that led to the establishment of stable density and thermal profiles (e.g. Mareschal & Jaupart, 2006).

The evidence for tectono-metamorphic processes in Archaean terranes is often obscured by polymetamorphic events, making it very difficult to read the rock record. Furthermore, we face an increasing scarcity of rock witnesses the further back in time we proceed. Structurally continuous sequences of the Mesoarchaean and earlier eras are relatively rare, increasing the potential for biased sampling. However, the infrequency of preserved Archaean complexes can be overcome by focusing on zircon grains, which are highly reliable archives of crust formation and differentiation processes. U–Pb dating in combination with oxygen or hafnium isotope analyses applied to single grains has been demonstrated to provide a unique tool for unravelling geodynamic processes for eras in Earth history from which all other records have been partially or completely eradicated (e.g. Wilde *et al.*, 2001; Pietranik *et al.*, 2008; Zeh *et al.*, 2008).

An unambiguous feature of intracrustal differentiation and cratonization is the generation of granitic magmas generated from the melting of sediments. Such an advanced step of crustal maturation is possible only when continental masses are large and stable enough to accommodate sedimentary basins, bury them and metamorphose them to high grades to cause crustal anatexis. Oxygen isotopes in zircon are ideal in tracing these processes, as they provide time-resolved information on the amount of recycled supracrustal materials in magmas when combined with U–Pb dating on single grains (Valley *et al.*, 2005; Kemp *et al.*, 2006, 2007).

Here, we present a zircon O–Hf isotope and U–Pb dating study from the Archaean Grunehogna Craton (GC) in East Antarctica, where outcrop is extremely scarce and the stratigraphic record is restricted. Despite these conditions, the record of the craton hidden in a handful of zircon grains is surprisingly detailed. Our combined stable and radiogenic isotope study of zircon demonstrates how geodynamic processes may be reconstructed for areas and eras for which the geological record is restricted to rare detrital or inherited grains in granites or clastic sediments.

GEOLOGY OF THE GRUNEHOGNA CRATON

The Grunehogna Craton (GC) in the Atlantic sector of East Antarctica is situated in western Dronning Maud Land (DML) between ~2 and 15°W at the Weddell Sea (Fig. 1). Palaeogeographical reconstructions and the ocean-floor spreading record show that it formed a fragment of or was adjacent to the Archaean to Palaeoproterozoic Kalahari Craton of southern Africa (the combined Kaapvaal and Zimbabwe Cratons with the Limpopo belt) that remained attached to Antarctica during the Jurassic breakup of Gondwana (e.g. Dietz & Sproll, 1970; Smith & Hallam, 1970; Martin & Hartnady, 1986; Groenewald *et al.*, 1991, 1995; Moyes *et al.*, 1993; Jacobs *et al.*, 1998, 2008*b*; Fitzsimons, 2000). Evidence for this reconstruction comes from a wealth of geochronological, palaeomagnetic, structural, petrological and geochemical data. It is also supported by reconstructions of ocean-floor spreading in the South Atlantic since the Jurassic (Martin & Hartnady, 1986). The complete separation of the Grunehogna from the Kalahari Craton was probably facilitated by large shear zones that were established by south-directed escape tectonics during the late Neoproterozoic assembly of Gondwana (Jacobs & Thomas, 2004).

The GC borders the high-grade metamorphic Maud Belt to the east and south (Fig. 1), which comprises meta-igneous and meta-sedimentary rocks metamorphosed at amphibolite- to granulite-facies grade during the Mesoproterozoic (1090–1060 Ma) 'Grenville' orogeny related to the assembly of the Rodinia supercontinent (Arndt *et al.*, 1991; Jacobs *et al.*, 2003*a*, 2008*b*; Board *et al.*, 2005; Bisnath *et al.*, 2006). Parts of the high-grade Maud Belt were reactivated in a second orogenic event in the late Neoproterozoic–early Phanerozoic (550–480 Ma) 'Panafrican' orogeny leading to the assembly of Gondwana (Groenewald *et al.*, 1995; Jacobs *et al.*, 2003*a*, 2003*b*, 2008*a*; Board *et al.*, 2005; Bisnath *et al.*, 2006). The timing and grade of metamorphism and associated magmatism strongly supports the above-mentioned palaeogeographical reconstruction. This reconstruction includes a correlation of the Maud Belt farther to the west into the Namaqua–Natal belt on the southern margin of the African Kalahari Craton and to the north into the Mozambique belt on the Kalahari Craton's eastern

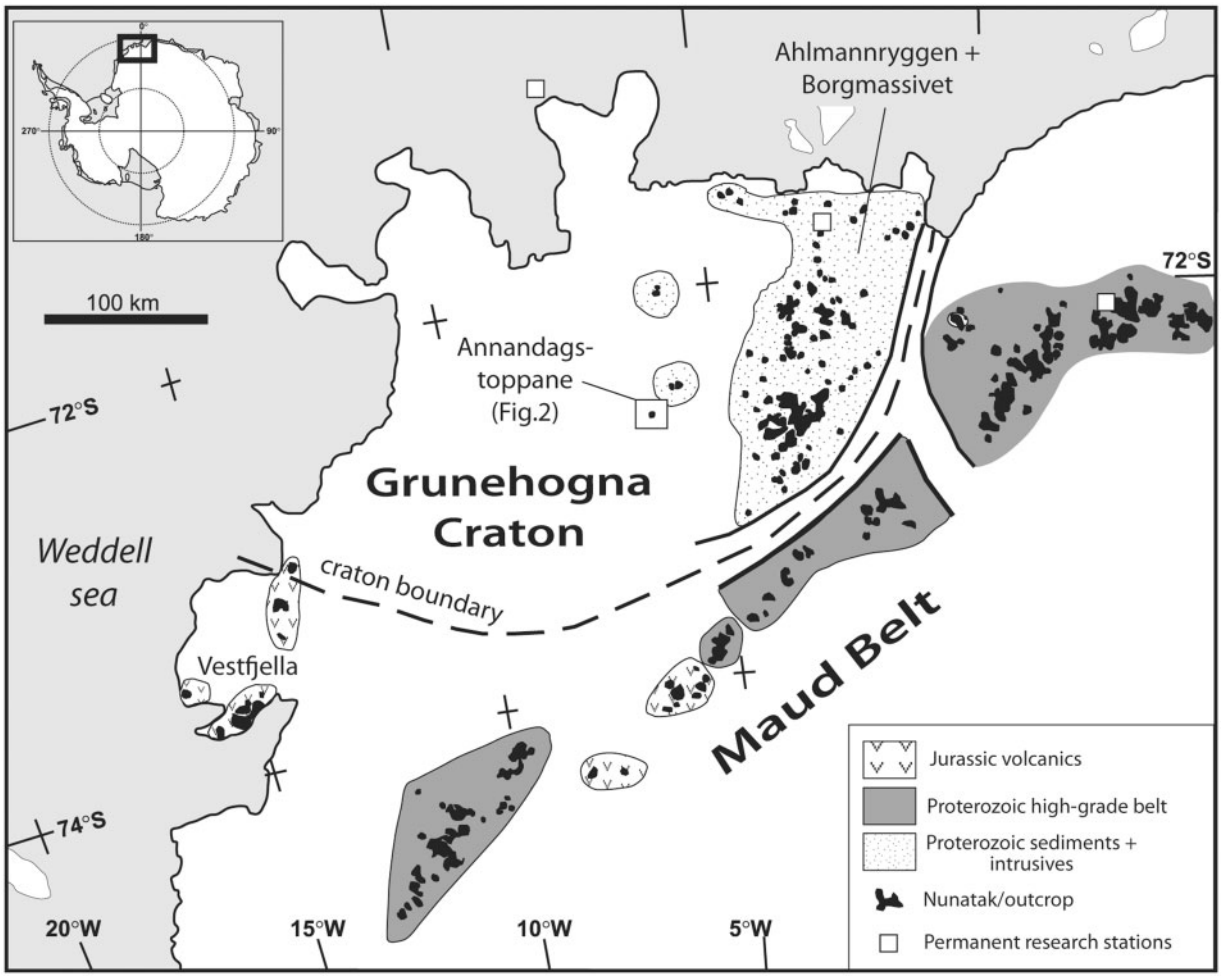

Fig. 1. Simplified map of Dronning Maud Land (DML) (modified after Board *et al.*, 2005). The major geological units are the high-grade metamorphic Maud Belt (Meso- and Neoproterozoic), the Mesoproterozoic sediments and sills in the Ritscherflya Supergroup (including Ahlmannryggen and Borgmassivet), and the Archaean basement of the Grunehogna craton (exclusively exposed at Annandagstoppane). The inset shows the Antarctic continent with the location of DML at the edge of the Weddell Sea.

margin (e.g. Arndt *et al.*, 1991; Groenewald *et al.*, 1991; Wareham *et al.*, 1998; Jacobs *et al.*, 2003*a*, 2008*b*).

West of the Pencksøkket–Jutulstraumen glaciers that separate the Maud Belt from the GC, the Ahlmannryggen and Borgmassivet nunataks comprise an ~2000 m thick pile of clastic and volcanic sediments of the Ritscherflya Supergroup (Wolmarans & Kent, 1982). These were deposited between 1130 and 1107 Ma in a shallow marine to braided river system (Wolmarans & Kent, 1982; Frimmel, 2004) and subsequently intruded by large (up to 400 m thick) mafic sills prior to diagenesis (Krynauw *et al.*, 1988; Curtis & Riley, 2003). The sills have an intrusion age of 1107 ± 2 Ma and have been correlated with the coeval mafic sills in the Umkondo region (Zimbabwe and Mozambique) and several other large mafic sills in the Kalahari craton, based on geochemistry, palaeomagnetism and intrusion age (e.g. Smith & Hallam, 1970; Martin & Hartnady, 1986; Powell *et al.*, 2001; Jones *et al.*, 2003; Frimmel, 2004; Hanson *et al.*, 2004, 2006; Grosch *et al.*, 2007).

The GC and its boundaries are almost completely covered by ice (Fig. 1). However, geophysical data (e.g. Golynsky & Aleshkova, 2000) and the occurrence of low-grade to non-metamorphic clastic and volcanic Mesoproterozoic sediments in the Ritscherflya Supergroup, which strongly contrast with the amphibolite- to granulite-facies rocks of the Maud Belt, strongly support the hypothesis of the distinct tectonic nature of the GC. This distinction is also evident in the radiogenic isotope characteristics of Phanerozoic mafic (sub-)volcanic rocks on the craton and in the Maud Belt, respectively (Grantham, 1996; Luttinen & Furnes, 2000; Leat *et al.*,

2005). Hence, it has been repeatedly demonstrated that the GC formed the eastern part of the Kalahari Craton—or at least was both similar and adjacent to it—for at least one billion years from the Mesoproterozoic to the Jurassic. However, because of the very scarce outcrop in Antarctica, a correlation of the cratonic basement itself has not been fully evaluated so far, and the Archaean to Palaeoproterozoic history of the GC and its possible connection to the well-investigated Kaapvaal Craton in that earlier period is unresolved.

Unfortunately, basement outcrops of the GC are almost absent and are limited to a small exposure of granite at Annandagstoppane (ADT; the 'Boxing Day Peaks'). Hence, this granite is of critical importance, as its precise age would provide a minimum age for the GC and allow for a correlation of its basement with the Kaapvaal Craton in the Palaeoproterozoic and the Archaean. Furthermore, the ADT granite forms the only West Gondwana exposure of Archaean rock in Antarctica (e.g. Boger & Miller, 2004), and therefore plays an important role in our understanding of Gondwana supercontinent assembly.

Attempts to date the crystallization of the granite have been made in the past in two studies by Halpern (1970) and Barton *et al.* (1987) using Rb–Sr mineral and whole-rock and Pb–Pb whole-rock methods. These studies derived Archaean ages of ~3·0 Ga with a number of younger events partly disturbing the isotope systems. Barton *et al.* (1987) demonstrated that temperatures in the ADT granite have remained below the closure temperature of the Rb–Sr isotope system in muscovite (~500°C) since the Mesoarchaean (2·8 Ga), demonstrating that this part of DML was indeed not strongly affected by the Grenvillian or Panafrican orogenies. However, Rb–Sr in biotite (~300°C) was reset in the Mesoproterozoic (~1150 Ma) and some hydrothermal activity dates to ~460 Ma. Zircon U–Pb ages had not been determined before this study, because of the scarcity and metamictization of zircon in the granite (Barton *et al.*, 1987).

The ADT granite is exposed only in three or four small nunataks (i.e. rock ridges sticking out of the ice) with a total outcrop area of $<0{\cdot}1\,km^2$ (Fig. 2). The outcrops comprise a dominantly leucocratic granite crosscut by garnet-bearing pegmatite dykes (Fig. 3a–c). Less common are darker varieties of biotite granite and granodiorite, biotite-rich enclaves (Fig. 3d) and Jurassic(?) basalt dykes. The granite is relatively fine grained (1–2 mm dominant grain size) and isotropic without any signs of ductile or brittle deformation. The boundaries between the darker and more leucocratic domains are continuous and no signs of single magma pulses or magma mingling were observed. The metre-scale pegmatite dykes cross-cut the granite with sharp contacts (Fig. 3a and c).

SAMPLES

The ADT locality was visited for 2 weeks in January 2008 by a two-man party (H.R.M. and S.T.B.) forming the British Antarctic Survey 2007–2008 field campaign in DML. The nunataks exposing the Mesoproterozoic gabbro and the Archaean granite were mapped using a global positioning system (GPS) and a US Geological Survey (USGS) satellite image (available via Google Earth). Sixteen rock samples from the granite outcrops were taken with a total weight of 67 kg, including several varieties of the granite, as well as samples from biotite-rich enclaves, garnet-bearing pegmatite and aplitic dykes and from the basalt dykes. Based on their appearance in hand specimen and thin section, six samples were selected for zircon separation and whole-rock chemical analyses (three granite samples, one granodiorite sample and two biotite-rich enclaves), as follows.

Z7-29-2 is the most leucocratic granite sample, consisting of quartz (Qtz), two feldspars (Fsp) and muscovite (Ms). No biotite or other mafic minerals are visible in hand specimen. The grain size is ~1 mm, and zircon is very rare. All separated zircon grains were dark orange to brown in transmitted light. No U–Pb dating was attempted on zircon from this sample.

Z7-29-7 is a fine-grained (1–2 mm) granite sample with only minor Ms, but larger K-feldspar (Ksp) megacrysts (5–10 mm). It is of darker appearance owing to a significant mode of fresh biotite (Bt) (Fig. 3f). Some zircon grains with non-metamict domains were extracted from this sample and successfully analysed and dated.

Z7-29-11 is a fine-grained Bt-bearing granite sample, which has fresh Bt and Fsp in some domains, but shows strong chloritization of Bt and sericitization of Fsp in others (Fig. 3e). Zircon is mostly altered and only very few grains were well enough preserved to be dated.

Z7-29-6 is a granodiorite sample with abundant Bt. A larger number of zircon grains were recovered from this sample, which produced near-concordant U–Pb ages.

Z7-29-10 is a sample of the Bt-rich enclaves, which form rounded or slightly angular dark domains in the pinkish granite. Boundaries between the two rock types are sharp in places, but continuous in others. In thin section, the rock shows an ophitic texture with Bt, Qtz and plagioclase (Pl) forming (semi-) euhedral inclusions in large, poikilitic Ksp (Fig. 3g). Zircon and apatite are included in the rock-forming minerals and are highly visible in biotite owing to the presence of intense radiation haloes. This sample produced a number of near-concordant zircon grains.

Z7-30-1 is another Bt-rich enclave. In contrast to Z7-29-10 it has a more equigranular texture formed by Bt, Ksp and Qtz with minor Ms (Fig. 3h) and Pl. Radiation haloes around accessory mineral inclusions in biotite are

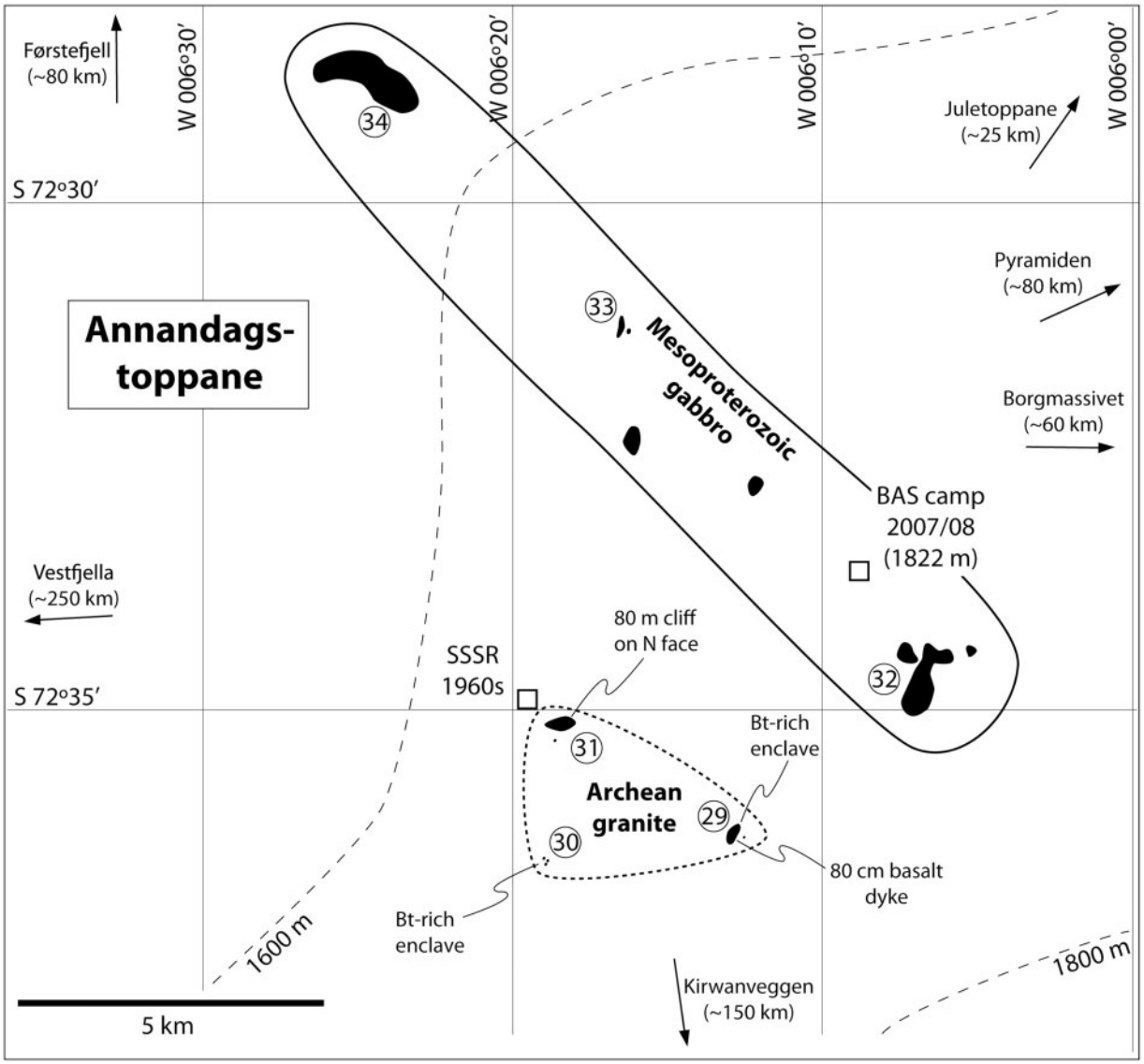

Fig. 2. Map of Annandagstoppane with sample stations marked by numbers. Rock outcrop is marked in black; everything else is occupied by snow-covered ice. The Archaean granite is exposed in three small nunataks in a restricted area in the southern part of Annandgstoppane, whereas the larger outcrops in the northern part are formed by Mesoproterozoic gabbro. No contact between the Mesoproterozoic gabbro and the Archaean granite is exposed. Latitudes, longitudes and distances to the nearest nunataks are given for orientation. The dashed lines are contour lines on the ice surface (metres above sea level).

also abundant in this sample, and a relatively large number of near-concordant zircon grains were recovered.

The typically magmatic microtextures displayed by both Bt-rich enclave samples, together with their high modes of feldspar, are taken as evidence that these rocks are cumulate fragments enclosed within the pluton, rather than xenoliths of metamorphic host-rock, melt residues or injections of mafic magma.

Most zircon grains separated from the samples are relatively dark or cloudy in transmitted light and show very weak cathodoluminescence (CL). Some grains, however, have relatively pristine central domains displaying slightly higher CL activity. These reveal oscillatory and sector zoning typical for magmatic zircon, and inherited cores in some cases (Fig. 4). The generally weak CL activity of the ADT zircons decreases from the core to rim of the grains, probably related to increasing U concentrations towards the rim. Almost all grains show brownish colours on their margins in transmitted light, correlated with a decrease in the CL signal. Analyses had to be focused on the least metamict domains with the higher CL activity.

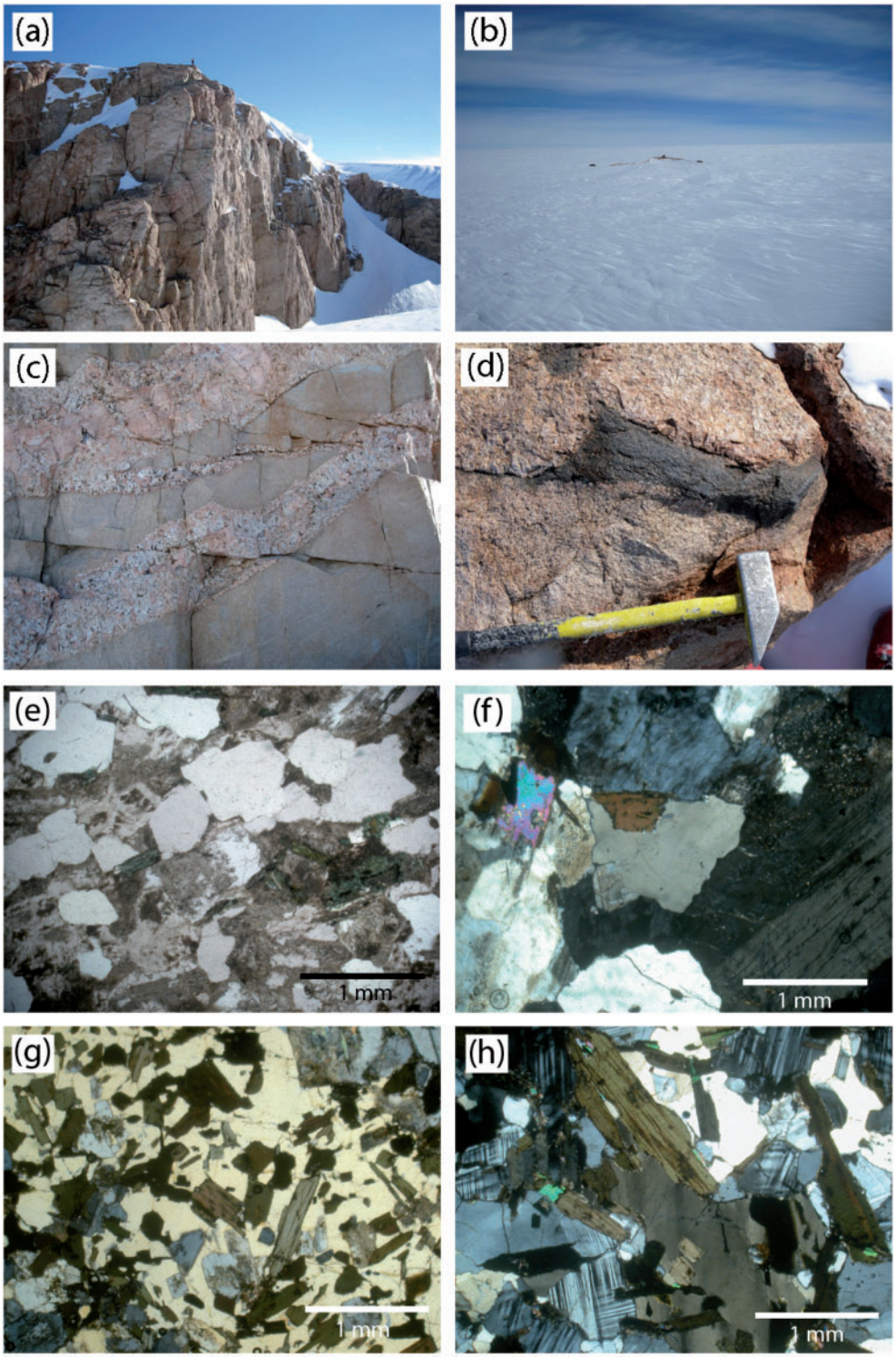

Fig. 3. The nunataks at ADT are very small, limited in number and separated by stretches of ice and snow. (a) Field image of an ~80 m high cliff at Station 31 (see Fig. 2) exposing the granite cross-cut by >5 m wide pegmatite dykes (note person for scale). This is by far the largest outcrop of the granite. (b) Field image of granite outcrop at Station 29, providing a good impression of the outcrop conditions at ADT (person and skidoos for scale). (c) Close-up of (a) showing coarse-grained garnet-bearing pegmatite (displaying graphic intergrowth of quartz and two feldspars) intruding biotite granite. Width of view ~2 m. (d) Biotite-rich enclave in granite (Station 29). The abundance of zircon in this cumulate sample is larger than in the host granite and metamictization is less intense. Width of view ~0·6 m. (e) Thin-section image of granite displaying effects of hydrothermal alteration with chlorite and sericite forming from biotite and feldspar. Quartz grains are clear (plane-polarized light; sample Z7-29-11). (f) Coarse-grained fraction of less-altered granite displaying orthoclase, plagioclase, quartz and biotite, as well as muscovite, which may or may not be primary magmatic (cross-polarized light; sample Z7-29-7). (g) Biotite-rich enclave displaying ophitic texture interpreted as a cumulate with quartz, plagioclase and abundant biotite cumulus grains and large orthoclase intercumulus (cross-polarized light; sample Z7-29-10). (h) Biotite-rich enclave showing unaltered feldspar, biotite and quartz with minor muscovite (cross-polarized light; sample Z7-30-1).

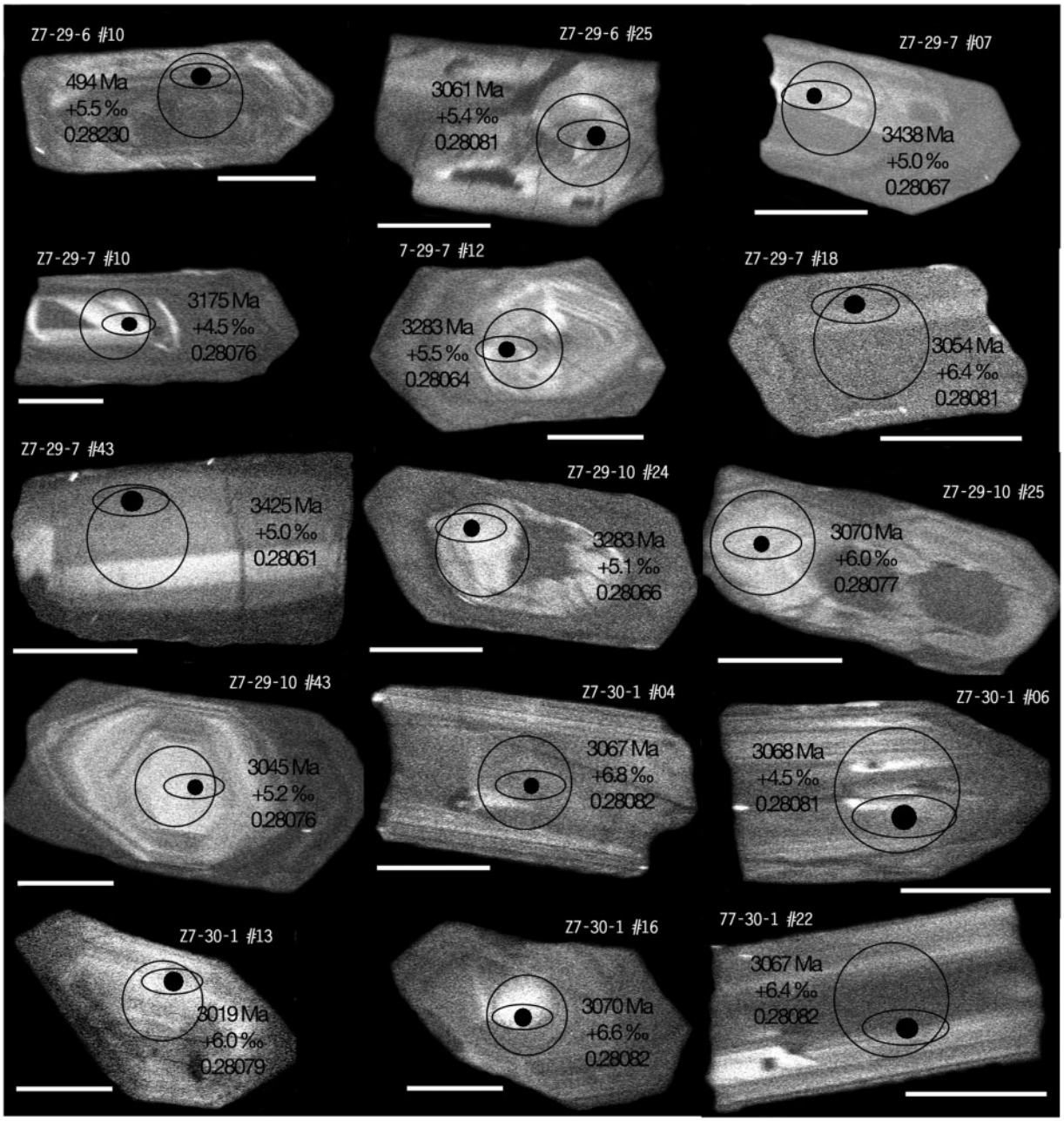

Fig. 4. Cathodoluminescence (CL) images of zircon grains separated from samples Z7-29-6 (granodiorite), Z7-29-7 (granite), Z7-29-l0 and Z7-30-1 (cumulate fragments). The images are of relatively poor quality because of low luminescence of the grains. Analytical spots are marked with black circles (SIMS O isotopes; 5–l0 μm spot size), open ovals (SIMS U–Pb dating; 30 μm long axis) and large open circles (laser Hf isotopes; ~40 μm spot size). Black numbers give the $^{207}Pb/^{206}Pb$ age, the $\delta^{18}O$ value and the initial $^{176}Hf/^{177}Hf$ ratio (calculated for the given age) for the spots on each grain. The white scale bars below each grain represent 50 μm.

ANALYTICAL METHODS

Whole-rock chemical compositions were determined by X-ray fluorescence (XRF) at Heidelberg (Germany), using fused glass discs for major elements and powder pellets for trace elements. Ten major and minor and l6 trace elements were determined using a Siemens® SRS303 X-ray spectrometer, equipped with a Rh-tube operated at 60 kV and 50 mA for the heavier elements and at 30 kV and 99 mA for the lighter elements. Precision and accuracy of the XRF analyses were controlled by using a range of international reference rock powders, and were ~0·5–1% for major elements and between 2 and l0% for trace

elements. Determination of loss on ignition (LOI) for each sample was performed using 1–1·5 g of powdered sample at 900°C.

A previous attempt by Barton *et al.* (1987) to separate zircon from ADT granite samples was unsuccessful because of the low modal zircon abundance and severe metamictization of most grains (Barton *et al.*, 1987). Therefore, we employed the novel technique of electric-pulse fragmentation (using SelFrag®) instead of a classical jaw crusher for the fragmentation of the rocks. This technique increases the recovery rate of zircon grains from a given amount of sample, and the grains are less fragmented and, hence, tend to be larger and euhedral. Also, grains with pristine cores and metamict rims (owing to U zoning) are preserved and not cracked and abraded, and can be hand-picked and their grain cores can be analysed by *in situ* methods. Heavy minerals in the samples were enriched by employing a Wilfley table, a magnetic separator and heavy liquids. Single zircons were than hand picked and mounted in epoxy and polished, together with grains of zircon reference materials 91500 and Temora-2 (Wiedenbeck *et al.*, 1995; Black *et al.*, 2004).

Cathodoluminescence was used as an imaging technique for the characterization of all grains for internal zoning and the degree of metamictization to select grains or domains of grains that were suitable for isotope analyses. The CL detector was attached to a Hitachi® scanning-electron microscope at the Department of Earth Sciences, University of Bristol.

Oxygen isotopic compositions of 65 zircon grains from five samples were determined by secondary ion mass spectrometry (SIMS) using the Cameca® IMS1270 multi-collector secondary-ion mass spectrometer ('ion microprobe') at the Edinburgh Materials and Micro-Analysis Centre (EMMAC; see Kemp *et al.*, 2007, for more analytical details) over a 1 day analytical session. Instrumental conditions were set with a 5·0 nA, nominally 10 kV $^{133}Cs^+$ primary beam focused to a 5–10 μm spot. An electron gun was used to neutralize surface charge. The 10 kV secondary beam resulted in count rates for ^{16}O of $\sim 2 \times 10^9\ s^{-1}$ and $\sim 4 \times 10^6\ s^{-1}$ for ^{18}O collected by dual Faraday cups. The internal precision of a single analysis was ≤0·3‰ (2σ). Oxygen isotopic compositions of samples are reported using the delta notation ($\delta^{18}O$ in ‰) relative to Vienna Standard Mean Ocean Water (VSMOW). Instrumental drift over the 14 h session (≤0·2‰, linear with time) was corrected by using blocks of five 91500 analyses before and after every 10–15 sample analyses. Spot-to-spot reproducibility on 91500 was ≤0·25‰. Instrumental mass fractionation was corrected by using reference zircon Temora-2 with $\delta^{18}O = +8{\cdot}20‰$ (Black *et al.*, 2004). Analytical accuracy is indicated by the results from 91500 relative to Temora-2, which deviated from the recommended value of $\delta^{18}O = +10{\cdot}07‰$ (Wiedenbeck *et al.*, 2004) by up to 0·7‰. At this stage it is unclear whether this discrepancy is caused by a matrix effect owing to lower HfO_2 concentrations in 91500 (0·66 wt %) compared with Temora-2 (0·98 wt %) (e.g. Peck *et al.*, 2001), or to the position of the grains on the sample mount (e.g. Ickert *et al.*, 2008). To minimize these potential effects, all samples were mounted within a 10 mm × 10 mm square in the centre of the mount with the reference zircons in the centre. HfO_2 concentrations of the samples vary between 0·88 and 1·40 wt % and were not corrected for a potential Hf-related matrix effect. The accuracy of the O isotope analyses presented in this study is estimated to ≤0·7‰.

U–Pb dating of zircon was carried out at EMMAC, also using the Cameca® IMS1270 ion microprobe. Analytical procedures are well established at EMMAC and were similar to those described by Schuhmacher *et al.* (1994) and Kelly *et al.* (2008). Twenty analytical cycles were acquired with the magnet cycling from the masses of HfO^+ to UO_2^+. A 5 nA, 12·5 kV mass filtered $^{16}O_2^-$ primary beam was focused to a 30 μm (long axis) elliptical spot. On sample and reference zircons the spot was centred onto the pits created by the Cs beam during O isotope analyses (Fig. 4). U/Pb ratios were calibrated against measurements of the 91500 reference zircon (1062·5 Ma; Wiedenbeck *et al.*, 1995). Sequences of 3–4 unknowns were bracketed by analyses of 91500 and Temora-2. Measurements over single sessions gave a standard deviation for the $^{207}Pb/^{206}Pb$ ratio of 91500 of 0·9% (95% confidence limit). Analyses of a secondary, external reference standard (Temora-2) during the analytical sessions yielded a mean $^{206}Pb/^{238}U$ age of 417·6 ± 3·5 Ma (95% confidence limit). Correction for *in situ* common Pb was made using measured ^{204}Pb counts and using the modern-day composition of common Pb. Uncertainty on this correction is included in the calculation of errors on the U/Pb and Pb/Pb ratios. Corrections for minor changes in beam density or energy were made based on the comparison of U/Pb with UO_2/UO ratios. Data were processed offline by R. W. Hinton (Edinburgh) using an in-house data reduction spreadsheet. Plots and age calculations were made using the ISOPLOT program (Ludwig, 2003).

The hafnium isotope compositions of 51 zircon grains were measured at the University of Bristol by multicollector inductively coupled plasma mass spectrometry (MC-ICP-MS) with a ThermoElectron® Neptune system. The same grains that were analysed for O isotopes and U–Pb dated on the ion probe were analysed for Hf isotopes by laser ablation-MC-ICP-MS at the identical spot sites (Fig. 4). A NewWave® 193 nm ArF laser was coupled to the Neptune system, and the methods and data reduction described by Hawkesworth & Kemp (2006) were employed. Ablation was conducted in He (flow rate $\sim 1{\cdot}3\ l\ min^{-1}$) mixed with argon ($\sim 0{\cdot}9\ l\ min^{-1}$) and

nitrogen (~0·005 l min^{-1}). The Hf isotope data were acquired using a 40 μm beam size with a fluence of ~6 mJ cm^{-2} and 4 Hz laser pulse repetition rate over a 60 s ablation period. This produced typical total Hf beams of 7, 10 and 11 V for proposed reference zircons Mud Tank, Temora-2 and Plešovice, respectively. Hf beams produced on samples varied from 5 to 11 V. Internal precision (2σ) varied between ±0·000016 and ±0·000039 for analyses of the reference materials and ±0·000022 and ±0·000052 for the samples. Long-term reproducibility (2σ) monitored on the reference zircons over several months was 77 ppm for Plešovice (n = 193), 75 ppm for Mud Tank (n = 80) and 109 ppm for Temora-2 (n = 85). All zircon laser ablation MC-ICP-MS analyses were adjusted relative to the JMC475 $^{176}Hf/^{177}Hf$ ratio of 0·282160 (e.g. Söderlund *et al.*, 2004).

Hafnium model ages were calculated using a ^{176}Lu decay constant $\lambda = 1{\cdot}867 \times 10^{-11}\,a^{-1}$ (Scherer *et al.*, 2001; Söderlund *et al.*, 2004), chondritic uniform reservoir (CHUR) $^{176}Lu/^{177}Hf = 0{\cdot}0336$ and $^{176}Hf/^{177}Hf = 0{\cdot}282785$ (Bouvier *et al.*, 2008) and depleted mantle (DM) $^{176}Lu/^{177}Hf = 0{\cdot}0384$ and $^{176}Hf/^{177}Hf = 0{\cdot}283250$ (Griffin *et al.*, 2002).

RESULTS

Whole-rock chemical compositions

The major element composition of samples from the main rock body ranges from granodioritic in the darker, more biotite-rich domains to granitic and almost haplo-granitic in the leucocratic, Ms-bearing portions, with SiO_2 contents increasing from ~68 to ~75 wt % (Table 1). Zirconium abundances decrease with increasing SiO_2 content from ~260 μg g^{-1} in the granodiorite to ~70 μg g^{-1} in the leucogranite. The Bt-rich enclaves show a strong enrichment in Fe, Mg, Ti und K and depletion in Si compared with the granite samples, in agreement with the high modal abundance of biotite. They are also enriched in most trace elements, including Zr with concentrations of several hundreds of μg g^{-1} (Table 1). Their enrichment in compatible elements, such as Cr, Ni and Co, supports their interpretation as cumulates.

The granodiorite and granite samples are moderately peraluminous with aluminium saturation indices [ASI = molar $Al_2O_3/(Na_2O + K_2O + CaO)$] between 1·02 and 1·21 and normative corundum (Table 1), in agreement with a minor mode of muscovite. Based on the Al-rich composition (ASI > 1) of the granite, the (rare) occurrence of monazite, the scarcity of zircon and a relatively high μ value ($^{238}U/^{206}Pb = 10{\cdot}8$) of its source, Barton *et al.* (1987) classified the ADT granite as S-type and concluded that it was possibly derived from melting of Archaean sediments in the crust.

U–Pb zircon data

A total of 62 zircon grains were analysed for their U and Pb isotopic compositions by SIMS. Many of these show discordant ages (Fig. 5), but a subset of 19 grains from the granite and granodiorite samples and 20 grains from the cumulate samples were less than 10% discordant, allowing for the calculation of precise and meaningful isotope ages (Table 2). U concentrations in the majority of these grains range from ~50 to 350 μg g^{-1}, with Th/U between 0·3 and 0·7 (Table 2). The largest group of zircon grains less than 5% discordant is formed by 21 grains (Fig. 5) defining a discordia with an upper intercept age of 3065 ± 12 Ma (95% confidence limit; MSWD = 0·34; probability of fit = 0·996). This group consists of 15 grains from the cumulates and six grains from the granite and granodiorite samples. Reducing the dataset to grains that are < 2% discordant and rejecting all analyses with a >5% deviation of the common-Pb corrected $^{208}Pb/^{206}Pb$ ratio from the same ratio predicted from Th/U (Table 2) leaves a group of 12 analyses (four granitoid + eight cumulate grains) defining an age of 3067·3 ± 8·2 Ma (2σ error including decay constant uncertainty; MSWD = 0·095; probability of concordance = 0·76). The grains from the plutonic samples completely overlap the grains from the cumulate samples at this age. The age 3067 ± 8 Ma is interpreted as the crystallization age for the major group of zircon in the ADT granite.

There are also a number of near-concordant grains (<5% discordance) with significantly older ages, which were mainly separated from the granite and granodiorite samples (Fig. 5). Four grains form an age group of 3433 ± 7 Ma, three grains form a group at 3279 ± 9 Ma and two other grains were dated to 3223 ± 4 Ma and 3175 ± 6 Ma (Table 2; Fig. 5). In addition, one zircon grain (~7% discordant) gave an age of ~500 Ma (Table 2).

Oxygen isotopic composition of zircon

The main group of near-concordant zircons (the 3067 Ma age group) ranges from +4·3 to +7·8‰ in $\delta^{18}O$, with the majority of the grains having values between +6 and +7‰ (Table 2; Fig. 6); that is, above the range of zircons crystallized from uncontaminated, ultimately mantle-derived, melts that have not interacted with the hydrosphere (Valley, 2003; Valley *et al.*, 2005; Hawkesworth & Kemp, 2006; Kemp *et al.*, 2006, 2007). Zircon grains from the cumulate samples overlap in the complete oxygen isotope range with zircon grains derived from the granite and granodiorite samples (Fig. 6).

Most of the older grains are indistinguishable from zircons crystallized from mantle-derived melts, or show slightly lower $\delta^{18}O$ values (Fig. 6). One ~3·2 Ga grain shows a value of +3·4 ± 0·3‰, which is significantly below the mantle array (Table 2). The O isotopic compositions of all grains are in a range that is considered typical

Table 1: Whole-rock major- and trace-element and normative compositions of Annandagstoppane samples

	This study						Barton *et al.* (1987)		
Type:	Bt-rich enclaves		Granodiorite	Granite			Granite		
Sample:	Z7-29-10	Z7-30-1	Z7-29-6	Z7-29-11	Z7-29-7	Z7-29-2	1*	2*	3*
Longitude W:	6°12·78′	6°18·56′	6°12·78′	6°12·78′	6°12·78′	6°12·44′			
Latitude S:	72°36·22′	72°36·55′	72°36·22′	72°36·22′	72°36·22′	72°36·26′			
Major elements (wt %)									
SiO_2	57·55	63·37	67·69	72·63	73·56	74·80	72·80	72·45	72·89
TiO_2	1·95	1·11	0·78	0·18	0·20	0·04	0·18	0·20	0·21
Al_2O_3	14·72	14·22	14·93	14·10	14·19	13·80	14·38	14·28	14·25
$Fe_2O_3^t$	11·94	8·51	4·78	1·41	1·38	0·58	1·58	1·75	1·58
MnO	0·24	0·17	0·12	0·05	0·04	0·01	0·02	0·02	0·01
MgO	3·45	1·85	1·31	0·39	0·35	0·05	0·46	0·55	0·47
CaO	1·52	0·46	1·28	0·84	1·08	0·43	1·28	1·25	1·32
Na_2O	3·14	2·14	4·83	3·99	4·22	4·46	4·57	4·31	4·01
K_2O	4·42	6·39	1·93	4·49	3·73	4·95	3·52	3·69	3·90
P_2O_5	0·43	0·13	0·06	0·04	0·07	0·02	0·06	0·07	0·06
LOI	1·63	1·56	1·70	1·11	0·98	0·77	1·03	1·06	0·94
Total	100·99	99·91	99·41	99·23	99·80	99·91	99·88	99·63	99·64
ASI	1·16	1·26	1·21	1·09	1·10	1·02	1·05	1·07	1·08
TA	7·56	6·53	6·76	8·48	7·95	9·41	8·09	8·00	7·91
CIPW norm									
Qtz	9·48	18·82	25·38	29·24	31·41	28·66	28·65	29·07	30·51
Or	26·12	37·76	11·41	26·53	22·04	29·25	20·80	21·81	23·05
Ab	26·57	18·11	40·87	33·76	35·71	37·74	38·72	36·47	33·93
An	4·73	1·43	5·96	3·91	4·90	2·00	5·96	5·74	6·16
Crn	3·04	3·26	2·71	1·24	1·41	0·37	0·86	1·09	1·18
En	8·59	4·61	3·26	0·97	0·87	0·12	1·15	1·37	1·17
Fs	12·52	9·38	5·06	1·60	1·51	0·70	1·76	1·95	1·70
Mag	2·60	1·85	1·04	0·31	0·30	0·13	0·34	0·38	0·34
Ilm	3·70	2·11	1·48	0·34	0·38	0·08	0·34	0·38	0·40
Ap	1·00	0·30	0·14	0·09	0·16	0·05	0·14	0·16	0·14
Trace elements ($\mu g\,g^{-1}$)									
Ba	477	281	179	740	493	88	406	561	558
Rb	489	503	269	209	173	300	165	168	192
Sr	144	54	160	130	170	43	156	173	217
Y	53	88	45	13	14	32	13	13	31
Zr	791	280	258	154	117	74	110	120	129
Nb	107	76	68	11	7	10	11	11	13
V	113	46	36	6	11	<5			
Cr	28	12	19	<10	<10	<10			
Co	26	11	10	<5	<5	<5			
Ni	18	6	7	3	4	<2			
Cu	22	7	28	<3	6	<3			
Zn	241	250	119	65	48	25			
Ga	39	35	32	17	17	19			
As	<5	<5	<5	<5	<5	<5			
Pb	14	25	23	21	26	31	31	30	32
Th	10	27	13	18	10	10			

Major elements were analysed by XRF. LOI, loss on ignition. $Fe_2O_3^t$, all Fe reported as trivalent Fe oxide. CIPW norm calculated assuming $FeO/(FeO + Fe_2O_3) = 0{\cdot}85$. ASI = molar $Al_2O_3/(Na_2O + K_2O + CaO)$. TA (total alkali) = $Na_2O + K_2O$. *Analyses from Barton *et al.* (1987) represent averages of analyses of several samples. Those researchers analysed a smaller number of trace elements.

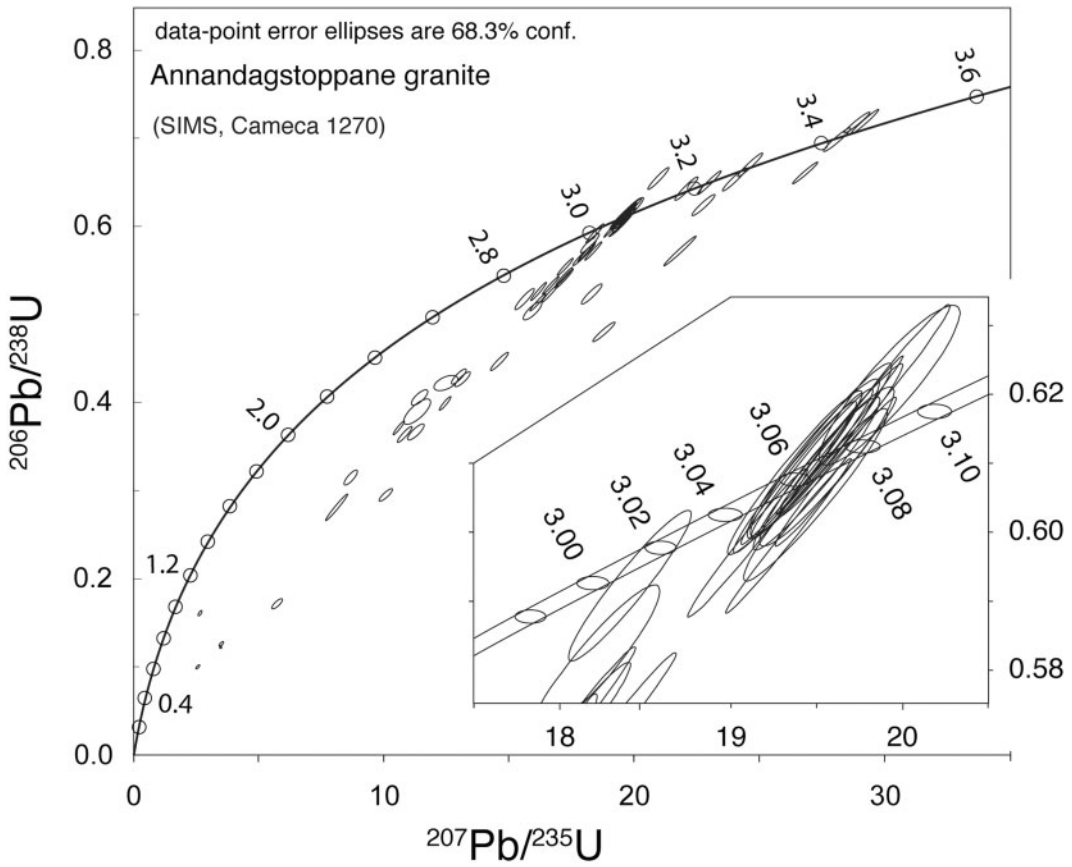

Fig. 5. U–Pb concordia diagram displaying results from 62 zircon grains from the ADT granite determined by SIMS at Edinburgh. The data form a rough discordant array between late Archaean and late Mesoproterozoic to early Phanerozoic. The most concordant points in the <3·1 Ga age group result in a concordance age of 3067 Ma (inset lower right). Older concordant ages are interpreted to represent inherited grains from the Palaeoarchaean host-rock or source of the granite.

for Archaean zircon as has been shown for granitoid and metasedimentary rocks from various localities (Valley *et al.*, 2005).

Hf isotopic composition of zircon

The 20 analyses of near-concordant zircons from the main group (the 3067 Ma age group) show a relatively small range in $^{176}Hf/^{177}Hf$, translating to εHf_t values between $-1{\cdot}8 \pm 1{\cdot}4$ and $+0{\cdot}7 \pm 1{\cdot}1$ (Table 3) with an average of $-0{\cdot}6 \pm 1{\cdot}7$. The value of 1·7 ε units for two standard deviations of the mean is close to the mean of the internal precisions of 1·2 ε units (2σ) of all analyses, showing that the group of samples is nearly homogeneous, and hence the magma was well mixed for Hf. Also, the cumulate samples display the same Hf isotope range as the granite and granodiorite samples in this age group. Zircon grains with elevated $\delta^{18}O$ values (>6·1‰) are not distinct in εHf_t from the group with mantle-like O isotope ratios at this age.

εHf_t values of some zircon grains in the oldest age group (~3·43 Ga) are highly positive and close to, or indistinguishable from, depleted mantle, whereas others in the same age group are 3–4 ε units below the depleted mantle (Table 3). Zircon grains in the intermediate age group plot onto or above the CHUR line, with the exception of one grain with very low $\delta^{18}O$ value, which has a negative εHf_t value (Fig. 7).

Hf model ages for separation of the crustal material from the depleted mantle were calculated for a crustal source composition with a $^{176}Lu/^{177}Hf$ ratio of 0·021. This relatively high value is slightly lower than the average $^{176}Lu/^{177}Hf$ ratio of Barberton komatiites (0·024; Blichert-Toft & Arndt, 1999; Blichert-Toft *et al.*, 2004) and accounts only for a minor portion of felsic material, such as tonalite–trondjemite–granodiorite (TTG) in the source region of the zircon-producing magmas. This assumption is based on the observation in the pre-3·1 Ga Archaean Kaapvaal Craton that most zircon-bearing magmatic rocks are granitoids of the TTG series that were generated from melting of mafic rather than felsic crust. Larger granite plutons generated from anatexis of felsic materials (i.e. from TTG or from sediments) appear only after ~ 3·14

Table 2: SIMS U–Pb zircon dating results and O isotope ratios of Annandagstoppane samples

Sample, grain no.	[U] ($\mu g\,g^{-1}$)	[Th] ($\mu g\,g^{-1}$)	[Pb] ($\mu g\,g^{-1}$)	[HfO_2] (wt %)	Th/U atomic	^{204}Pb ($ng\,g^{-1}$)	$^{206}Pb^*/^{238}U$ (1σ)	$^{207}Pb^*/^{235}U$ (1σ)	$^{207}Pb^*/^{206}Pb^*$ (1σ)	$^{206}Pb/^{238}U$ age (Ma)	$^{207}Pb/^{235}U$ age (Ma)	$^{207}Pb/^{206}Pb$ age (Ma)	Disc. (%)	Th disc. (%)†	$\delta^{18}O$ (‰), (2σ)
Granodiorite															
Z7-29-6															
2	125	60	94	1·18	0·49	6·9	0·6241 (79)	22·72 (30)	0·2640 (10)	3126 (31)	3215 (13)	3270 (6)	−4·4	−2·6	+4·7 (2)
4	191	238	170	1·02	1·27	3·2	0·6544 (83)	20·94 (27)	0·2320 (6)	3245 (32)	3136 (13)	3066 (4)	5·8	3·0	+6·2 (2)
10	646	422	56	1·12	0·67	6·7	0·0797 (10)	0·637 (9)	0·0580 (4)	494 (6)	501 (6)	530 (15)	−6·8	0·5	+5·5 (2)
11	162	83	99	0·94	0·53	207	0·5171 (78)	15·59 (25)	0·2187 (13)	2687 (33)	2852 (15)	2971 (9)	−9·6	−9·2	+5·0 (2)
15	94	53	66	0·91	0·58	14·2	0·5810 (74)	18·20 (25)	0·2272 (12)	2953 (30)	3000 (13)	3032 (9)	−2·6	−2·7	+6·0 (2)
18	146	68	114	1·08	0·48	2·9	0·6499 (83)	22·96 (30)	0·2563 (6)	3228 (33)	3225 (13)	3223 (4)	0·1	−5·3	+3·4 (3)
21	645	218	387	1·07	0·35	32·0	0·5265 (67)	16·16 (21)	0·2226 (4)	2727 (28)	2886 (12)	2999 (3)	−9·1	−0·5	+5·9 (2)
22	88	41	77	1·11	0·48	1·7	0·7150 (93)	28·80 (39)	0·2921 (10)	3477 (35)	3447 (13)	3428 (6)	1·4	1·3	+5·7 (2)
25	62	36	46	0·92	0·60	2·2	0·6121 (83)	19·53 (27)	0·2314 (8)	3078 (33)	3068 (13)	3061 (6)	0·6	2·2	+5·4 (3)
30	234	141	212	1·17	0·62	1·8	0·7190 (90)	29·16 (37)	0·2942 (6)	3492 (34)	3459 (12)	3439 (4)	1·6	−1·8	+4·2 (3)
34	191	58	131	1·20	0·31	7·8	0·5994 (74)	19·33 (24)	0·2339 (4)	3027 (30)	3059 (12)	3079 (2)	−1·7	0·1	+5·4 (2)
35	101	35	70	1·40	0·35	2·3	0·6087 (79)	19·37 (26)	0·2308 (8)	3065 (31)	3061 (13)	3057 (6)	0·3	0·8	+7·8 (2)
Granite															
Z7-29-7															
7	92	48	76	1·15	0·53	7·5	0·6611 (83)	26·80 (34)	0·2939 (6)	3272 (32)	3376 (12)	3438 (3)	−4·8	3·0	+5·0 (1)
10	118	87	95	0·97	0·76	1·8	0·6429 (81)	22·03 (29)	0·2486 (9)	3200 (32)	3185 (13)	3175 (6)	0·8	−1·9	+4·5 (2)
12	104	41	83	1·26	0·41	1·8	0·6700 (85)	24·59 (32)	0·2662 (8)	3306 (33)	3292 (13)	3283 (5)	0·7	−4·9	+5·5 (2)
18	342	310	238	0·97	0·93	80·5	0·5410 (73)	17·18 (24)	0·2303 (6)	2787 (30)	2945 (13)	3054 (4)	−8·7	20·9	+6·4 (2)
43	66	33	57	0·90	0·51	1·0	0·6987 (88)	28·08 (37)	0·2915 (10)	3416 (33)	3422 (13)	3425 (5)	−0·3	−0·2	+5·0 (2)
Z7-29-11															
12	193	43	132	1·28	0·23	3·2	0·6088 (72)	19·61 (23)	0·2336 (5)	3065 (29)	3072 (11)	3076 (4)	−0·3	−1·1	+7·0 (2)
24	86	39	61	1·26	0·46	36·4	0·6055 (83)	19·49 (28)	0·2335 (9)	3052 (33)	3067 (14)	3076 (6)	−0·8	−0·4	+5·9 (1)
Biotite-rich enclaves															
Z7-29-10															
14	242	110	163	1·02	0·47	14·8	0·5730 (68)	18·11 (22)	0·2292 (5)	2920 (28)	2996 (12)	3046 (4)	−4·1	−2·4	+5·9 (2)
24	34	15	26	1·17	0·45	1·9	0·6533 (83)	23·98 (31)	0·2662 (9)	3241 (32)	3267 (13)	3283 (5)	−1·3	5·6	+5·1 (2)
25	46	29	34	1·05	0·65	1·3	0·6212 (76)	19·92 (27)	0·2326 (13)	3115 (30)	3088 (13)	3070 (9)	1·5	−1·2	+6·0 (3)
39	189	175	146	0·96	0·95	16·4	0·5984 (71)	19·09 (23)	0·2314 (5)	3023 (29)	3047 (12)	3062 (3)	−1·3	−2·6	+6·4 (2)
43	63	33	42	1·10	0·55	19·9	0·5660 (69)	17·88 (23)	0·2291 (7)	2891 (28)	2983 (12)	3045 (5)	−5·0	−1·1	+5·2 (2)
45	342	99	215	1·15	0·30	78·4	0·5542 (65)	17·22 (20)	0·2253 (5)	2843 (27)	2947 (11)	3019 (3)	−5·8	9·7	+5·6 (3)
47	198	133	132	1·00	0·69	49·1	0·5430 (66)	17·17 (22)	0·2294 (8)	2796 (28)	2945 (12)	3047 (6)	−8·2	3·9	+6·3 (2)
Z7-30-1															
4	105	61	78	0·90	0·59	1·0	0·6135 (73)	19·64 (24)	0·2322 (6)	3084 (29)	3074 (12)	3067 (4)	0·5	−0·8	+6·8 (2)
6	90	57	67	0·92	0·65	1·0	0·6086 (73)	19·50 (24)	0·2324 (8)	3064 (29)	3067 (12)	3068 (6)	−0·1	−0·9	+4·5 (3)
7	85	32	60	1·34	0·39	1·1	0·6100 (72)	19·47 (24)	0·2315 (6)	3070 (29)	3065 (12)	3062 (4)	0·3	−2·1	+7·2 (2)
12	154	116	117	0·93	0·77	2·5	0·6081 (73)	19·37 (24)	0·2311 (6)	3062 (29)	3061 (12)	3059 (4)	0·1	−0·9	+4·3 (4)
13	41	14	28	0·95	0·35	0·0	0·5923 (72)	18·41 (24)	0·2254 (9)	2999 (29)	3011 (12)	3019 (7)	−0·7	−6·8	+6·0 (2)
15	178	96	113	1·28	0·56	4·1	0·5332 (69)	16·64 (22)	0·2263 (5)	2755 (29)	2914 (13)	3026 (3)	−9·0	−10·1	+7·4 (2)
16	63	21	44	0·97	0·34	0·6	0·6096 (76)	19·56 (26)	0·2327 (10)	3068 (30)	3070 (13)	3070 (7)	−0·1	−0·2	+6·6 (4)
19	178	88	120	1·07	0·51	6·0	0·5708 (68)	18·08 (22)	0·2297 (7)	2911 (28)	2994 (12)	3049 (5)	−4·5	−4·3	+7·7 (3)
21	59	30	42	0·91	0·53	1·1	0·6108 (76)	19·48 (26)	0·2313 (9)	3073 (30)	3066 (13)	3061 (6)	0·4	−1·0	+6·6 (3)
22	115	73	87	0·89	0·65	0·4	0·6218 (73)	19·91 (24)	0·2323 (5)	3117 (29)	3087 (11)	3067 (4)	1·6	−1·8	+6·4 (2)
23	355	170	257	1·03	0·49	1·6	0·6141 (76)	19·63 (25)	0·2319 (3)	3087 (30)	3074 (12)	3065 (1)	0·7	−0·4	+7·3 (2)
32	174	113	129	0·88	0·66	1·5	0·6092 (72)	19·41 (23)	0·2311 (5)	3067 (29)	3062 (12)	3059 (3)	0·3	−3·1	+6·0 (2)
33	223	132	154	0·97	0·61	9·0	0·5723 (67)	18·35 (22)	0·2325 (5)	2917 (28)	3008 (11)	3069 (3)	−4·9	1·5	+6·8 (3)

†Discrepancy between the corrected $^{208}Pb/^{206}Pb$ ratio and the same ratio as predicted from the $^{232}Th/^{238}U$ ratio for the $^{207}Pb/^{206}Pb$ age.
Only analyses that were less than ±15% discordant are listed.

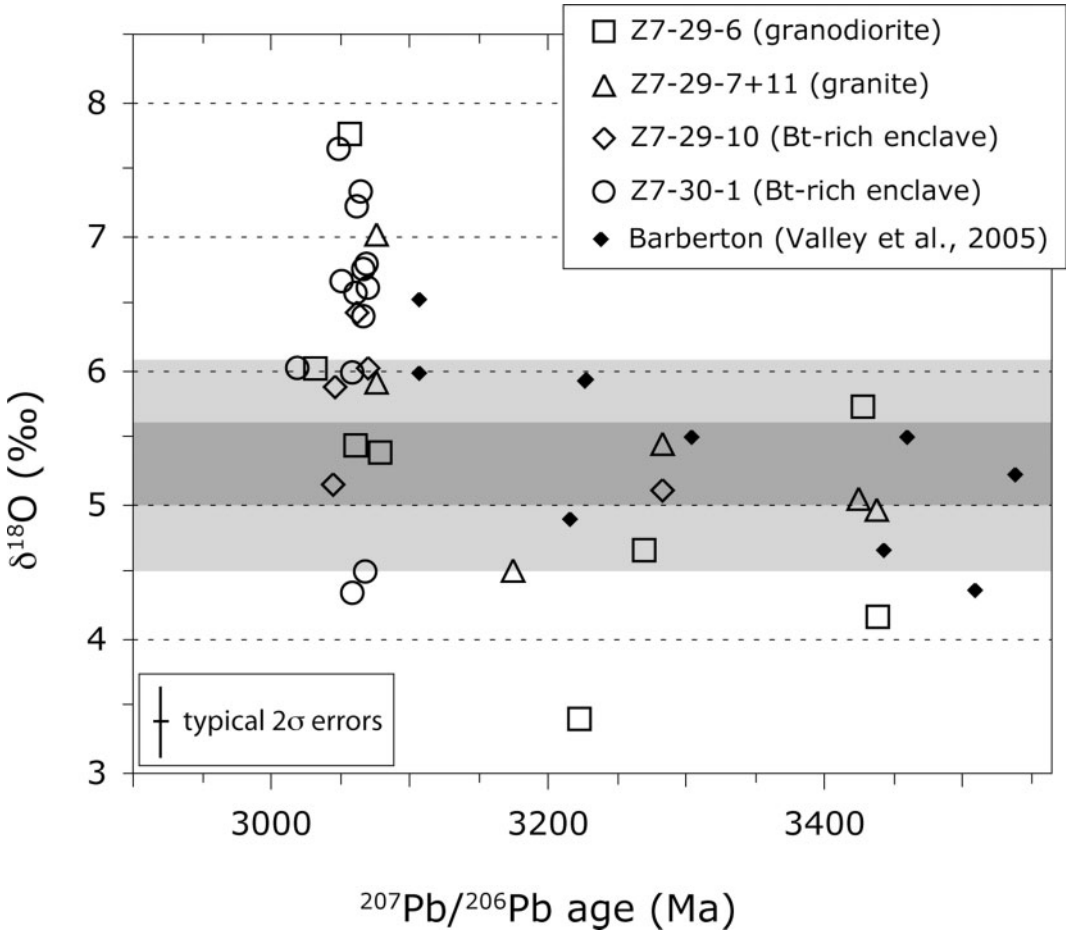

Fig. 6. Oxygen isotopic composition plotted versus the $^{207}Pb/^{206}Pb$ ages of single zircon grains from ADT (<5% discordant grains only). The dark grey field marks the O isotope ratios ($\delta^{18}O = 5{\cdot}3 \pm 0{\cdot}3‰$) of mantle-derived zircon (Valley *et al.*, 2005), whereas zircon outside the light grey fields crystallized from melts with a sedimentary or hydrothermally altered component. Within the light grey fields, the limited precision and accuracy of the method does not allow for such a distinction. For comparison, zircon data from granites and tonalites from the Barberton area (South Africa) are plotted (Valley *et al.*, 2005).

Ga, and can therefore be neglected in a discussion on crustal evolution in this case. Hf model ages for a felsic magma source ($^{176}Lu/^{177}Hf = 0{\cdot}015$) are given in Table 3 for comparison. Assuming a lower $^{176}Lu/^{177}Hf$ ratio of 0·015 decreases the model ages (T_{DM}) by ~150 Myr for the 3067 Ma age group, but it has no impact on the general conclusions presented in this study, nor on the discussion below.

Two of the oldest zircon grains in the ADT granite have εHf_t values close to the depleted mantle line, and consequently, their T_{DM} ages are close to or indistinguishable from their crystallization age. However, other grains in the same age group with significantly lower εHf_t values have higher T_{DM} ages of ~3·75 Ga, showing that the ADT granite contains contributions from at least two crustal components. All >3·1 Ga zircon grains produce model ages that can be subdivided into these two groups defined by the oldest grains, and require different crustal sources separated from the depleted mantle at ~3·50 Ga and at ~3·75 Ga, respectively.

Hf model ages of all grains in the 3067 Ma age group are intermediate between the groups defined by the older grains (Fig. 7) with a mean T_{DM} of ~3·68 Ga. The one apparently young zircon grain (No. Z7-29-6-10) with a near-concordant U–Pb age of ~500 Ma has a much more radiogenic Hf isotopic composition ($^{177}Hf/^{176}Hf = 0{\cdot}282298$; Table 3). Its U–Pb age is close to the age of chloritization and hydrothermal activity that affected parts of the granite (Barton *et al.*, 1987). The zircon is, hence, best interpreted as a grain recrystallized during that hydrothermal activity, which apparently gained some radiogenic Hf from the rock matrix. A Hf model age for this grain is therefore considered geologically meaningless and the grain is not be discussed further.

Table 3: Hafnium isotope data of zircon from Annandagstoppane samples determined by LA-MC-ICP-MS

Sample, grain no.	Age (Ma; 2σ)	Disc. (%)	$^{176}Lu/^{177}Hf$	$^{176}Yb/^{177}Hf$	$^{176}Hf/^{177}Hf$ (present)	$^{176}Hf/^{177}Hf_t$ (initial; 2σ)	εHf_t (initial; 2σ)	T_{DM} (Ma) felsic	mafic	$\delta^{18}O$ (‰; 2σ)
Granodiorite										
Z7-29-6										
2	3270 (12)	−4·4	0·00086	0·0253	0·280732	0·280678 (28)	+0·3 ± 1·0	3623	3744	+4·7 (2)
4	3067 (8)*	5·8	0·00170	0·0457	0·280899	0·280798 (29)	−0·2 ± 1·0	3497	3644	+6·2 (2)
10	494 (12)	−6·8	0·00122	0·0351	0·282309	0·282298 (30)	−6·2 ± 1·1	1841	2298	+5·5 (2)
11	3067 (8)*	−9·6	0·00200	0·0607	0·280927	0·280809 (43)	+0·2 ± 1·5	3471	3610	+5·0 (2)
15	3067 (8)*	−2·6	0·00195	0·0537	0·280880	0·280765 (35)	−1·4 ± 1·3	3572	3745	+6·0 (2)
18	3223 (8)	0·1	0·00252	0·0660	0·280778	0·280621 (34)	−2·8 ± 1·2	3786	3978	+3·4 (3)
22	3428 (12)	1·4	0·00101	0·0279	0·280777	0·280710 (31)	+5·2 ± 1·1	3432	3434	+5·7 (2)
25	3067 (8)*	0·6	0·00125	0·0332	0·280885	0·280811 (31)	+0·2 ± 1·1	3467	3604	+5·4 (3)
30	3439 (8)	1·6	0·00150	0·0387	0·280699	0·280600 (34)	+1·5 ± 1·2	3676	3758	+4·2 (3)
34	3067 (8)*	−1·7	0·00129	0·0340	0·280828	0·280752 (41)	−1·8 ± 1·4	3601	3783	+5·4 (2)
35	3067 (8)*	0·3	0·00056	0·0162	0·280810	0·280777 (37)	−1·0 ± 1·3	3545	3708	+7·8 (2)
Granite										
Z7-29-7										
7	3438 (6)	−4·8	0·00130	0·0343	0·280757	0·280671 (22)	+4·0 ± 0·8	3515	3542	+5·0 (1)
10	3175 (12)	0·8	0·00212	0·0546	0·280894	0·280764 (36)	+1·1 ± 1·3	3496	3607	+4·5 (2)
12	3283 (10)	0·7	0·00087	0·0201	0·280693	0·280638 (24)	−0·8 ± 0·8	3704	3848	+5·5 (2)
18	3067 (8)*	−8·7	0·00112	0·0319	0·280876	0·280810 (52)	+0·2 ± 1·9	3469	3607	+6·4 (2)
43	3425 (10)	−0·3	0·00090	0·0203	0·280668	0·280609 (32)	+1·5 ± 1·1	3666	3749	+5·0 (2)
Z7-29-11										
12	3067 (8)*	−0·3	0·00094	0·0243	0·280843	0·280788 (29)	−0·6 ± 1·0	3521	3676	+7·0 (2)
24	3067 (8)*	−0·8	0·00059	0·0161	0·280855	0·280821 (26)	+0·6 ± 0·9	3446	3576	+5·9 (1)
Biotite-rich enclaves										
Z7-29-10										
14	3067 (8)*	−4·1	0·00163	0·0410	0·280863	0·280767 (28)	−1·3 ± 1·0	3568	3740	+5·9 (2)
24	3283 (10)	−1·3	0·00029	0·0076	0·280678	0·280660 (29)	−0·0 ± 1·0	3654	3782	+5·1 (2)
25	3067 (8)*	1·5	0·00125	0·0345	0·280846	0·280773 (37)	−1·1 ± 1·3	3555	3722	+6·0 (3)
39	3067 (8)*	−1·3	0·00203	0·0538	0·280905	0·280785 (38)	−0·7 ± 1·3	3526	3684	+6·4 (2)
3	3067 (8)*	−5·0	0·00159	0·0396	0·280853	0·280759 (32)	−1·6 ± 1·1	3586	3763	+5·2 (2)
45	3067 (8)*	−5·8	0·00085	0·0210	0·280833	0·280783 (23)	−0·8 ± 0·8	3532	3691	+5·6 (3)
47	3067 (8)*	−8·2	0·00129	0·0326	0·280866	0·280790 (42)	−0·5 ± 1·5	3516	3670	+6·3 (2)
Z7-30-1										
4	3067 (8)*	0·5	0·00305	0·0764	0·281002	0·280822 (31)	+0·6 ± 1·1	3442	3571	+6·8 (2)
6	3067 (8)*	−0·1	0·00231	0·0608	0·280942	0·280806 (41)	+0·1 ± 1·5	3480	3621	+4·5 (3)
7	3067 (8)*	0·3	0·00090	0·0234	0·280837	0·280784 (32)	−0·7 ± 1·2	3530	3688	+7·2 (2)
12	3067 (8)*	0·1	0·00250	0·0633	0·280902	0·280755 (32)	−1·7 ± 1·1	3594	3774	+4·3 (4)
13	3067 (8)*	−0·7	0·00228	0·0605	0·280955	0·280821 (33)	+0·6 ± 1·2	3446	3576	+6·0 (2)
15	3067 (8)*	−9·0	0·00101	0·0259	0·280831	0·280772 (25)	−1·2 ± 0·9	3557	3725	+7·4 (2)
16	3067 (8)*	−0·1	0·00130	0·0330	0·280899	0·280823 (31)	+0·7 ± 1·1	3440	3568	+6·6 (4)
19	3067 (8)*	−4·5	0·00109	0·0288	0·280855	0·280791 (26)	−0·5 ± 0·9	3513	3666	+7·7 (3)
21	3067 (8)*	0·4	0·00203	0·0509	0·280908	0·280789 (30)	−0·6 ± 1·1	3519	3673	+6·6 (3)
22	3067 (8)*	1·6	0·00269	0·0668	0·280974	0·280816 (32)	+0·4 ± 1·1	3457	3590	+6·4 (2)
23	3067 (8)*	0·7	0·00197	0·0512	0·280914	0·280798 (31)	−0·2 ± 1·1	3497	3644	+7·3 (2)

*Zircon grains with $^{207}Pb/^{206}Pb$ ages <3080 Ma were assumed to represent grains crystallized during the emplacement and crystallization of the granite pluton at 3067 ± 8 Ma.
Hf model ages are given for a felsic and a mafic magma source with $^{176}Lu/^{177}Hf$ ratios of 0·015 and 0·021, respectively.

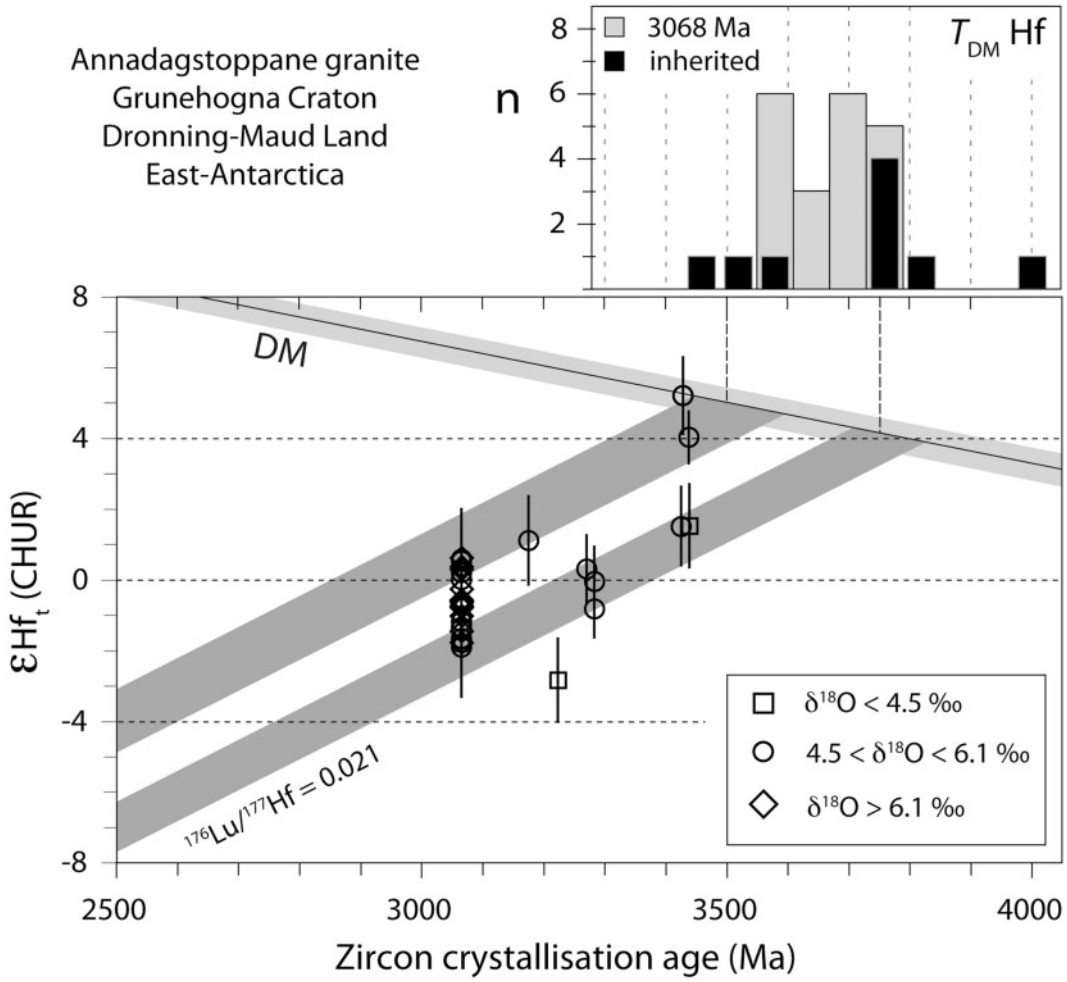

Fig. 7. Hf isotopic evolution of the ADT granite, including samples from the Bt-rich cumulates. Only zircon grains that are <5% discordant are plotted. All zircon grains with $^{207}Pb/^{206}Pb$ ages <3080 Ma were assumed to represent grains crystallized during the emplacement and crystallization of the granite pluton at 3067 ± 8 Ma. It should be noted that zircons from the three O isotope groups completely overlap in εHf in the 3067 Ma group. Hf evolution and Hf model ages (T_{DM}) were calculated for a mafic crustal source ($^{176}Lu/^{177}Hf = 0{\cdot}021$). Upper panel: histogram of Hf model ages (bin width 60 Ma); whereas the inherited grains form two groups at 3·50 Ga and at 3·75 Ga, the 3067 Ma age group shows little variation and Hf model ages intermediate between the two inherited groups.

DISCUSSION

Crystallization age of the ADT granite

The dominant group of zircons with a crystallization age of 3067 ± 8 Ma is interpreted to define the crystallization age of the ADT granite. Younger grains show discordance and/or disturbed $^{208}Pb/^{206}Pb$ ratios, probably reflecting metamictization, hydrothermal recrystallization or Pb loss. Older grains ranging from 3175 ± 6 Ma to 3433 ± 7 Ma are interpreted as grains inherited from the crustal source region of the magma or from the wall-rock of the granite intrusion. The crystallization age determined from U–Pb zircon dating in this study is compatible with ages of 2960 ± 80 Ma [$\lambda(^{87}Rb) = 1{\cdot}42 \times 10^{-11}\,a^{-1}$] and 2945–3115 Ma for the ADT granite determined in the earlier Rb–Sr and Pb–Pb geochronology studies (Halpern, 1970; Barton *et al.*, 1987). The thermal event that caused a partial homogenization of Sr isotopes on the whole-rock scale at ~2820 Ma (Barton *et al.*, 1987) may have caused a first partial Pb loss in some zircon grains at that time. This may have produced the near-concordant ages below the proposed crystallization age. Most grains, however, define discordia intersecting the concordia at the proposed crystallization age or the age of the inherited grains on their upper intercepts and between ~1·1 Ga and ~0·45 Ga on their lower intercepts. Hence, they do not show recent Pb loss, but Pb loss possibly related to the hydrothermal processes that apparently affected the granite in the Mesoproterozoic and in the Cambro-Ordovician (Barton *et al.*, 1987).

Sedimentary magma source

The Al-rich composition of the ADT granite, together with other geochemical and petrological characteristics, has been taken as evidence for a metasedimentary crustal source and its classification as a S-type granite (Barton *et al.*, 1987). This hypothesis is strongly supported by the elevated $\delta^{18}O$ values of zircon (Fig. 6). The oxygen isotopic compositions of the 3067 Ma zircon grains are elevated, with most $\delta^{18}O$ values between +6 and +7‰, which reflects a contribution of material to the magma that has interacted with the hydrosphere (Valley, 2003; Valley *et al.*, 2005). The granitic magma, therefore, must have been generated from melting of metasediments in the middle or lower crust, or at least must have assimilated significant amounts of (meta-)sediment during its ascent or emplacement (see Kemp *et al.*, 2007). Based on the age of the youngest inherited grain, the sediment that was the source for or contributed to the ADT granite magma must have been deposited after 3175 Ma.

The evolution from the mantle-like values of the pre-3·15 Ga grains to higher $\delta^{18}O$ values in the younger grains is a trend that is also apparent in TTG zircons from the Barberton Mountain Land in the Kaapvaal Craton (Fig. 6; Valley *et al.*, 2005). Although the number of analysed >3·1 Ga zircon grains is limited, the data strongly suggest that involvement of weathered material in the generation of magmatic rocks in the GC and Kaapvaal Craton was insignificant in the Palaeo- and Eoarchaean, but became important after 3·15 Ga. Thus, in the GC the early Mesoarchaean may mark a transition towards significant intracrustal recycling and sediment melting. For the Kaapvaal Craton this process of crustal maturation has been documented in much greater detail based on the appearance of large potassic granite plutons and batholiths at ~3·1 Ga, instead of the earlier TTG-type intrusions (e.g. Poujol *et al.*, 2003; Schoene *et al.*, 2008).

Zircon comparison with the Kaapvaal Craton

For a more detailed assessment of an Archaean link of the GC to the Kaapvaal Craton, the Eo- to Mesoarchaean evolution of the African domains need to be briefly summarized here. The well-established plate tectonic reconstruction of Africa–Antarctica in Gondwana places the GC in a position close to the southeastern African coast at the southern end of Mozambique (Fig. 8). This palaeogeographical position shrinks the distance between the ADT granite and the Archaean of the Swaziland and Witwatersrand Blocks to a mere 300 km (Fig. 8).

The African Kalahari Craton is subdivided into the Zimbabwe Craton in the north and the Kaapvaal Craton in the south, separated by the Limpopo Belt (Fig. 8). These three cratonic blocks were separated by oceanic basins in the earlier Archaean and were amalgamated only in the Neoarchaean at 2·7–2·6 Ga (e.g. van Reenen *et al.*, 1987; de Wit *et al.*, 1992; Zeh *et al.*, 2009). Hence, for the Archaean Grunehogna–Kaapvaal connection related to the Mesoarchaean ADT granite, the Limpopo Belt and Zimbabwe Craton have no bearing. The Kaapvaal Craton itself was assembled from various terranes: (1) the Swaziland Block (SB; Fig. 8), which is exposed in the southern part of the Barberton Mountain Land and in the Ancient Gneiss Complex (AGC) of Swaziland; (2) the Witwatersrand Block (WB), which is exposed between the Barberton and the Murchison greenstone belts and in various domes in the Witwatersrand basin; (3) the Kimberley Block in the west; (4) the Pietersburg Block (PB) in the north, which comprises, for example, the Giyani greenstone belt and related TTG and granite plutons. The SB and WB collided at ~3·23 Ga (Poujol *et al.*, 2003; Schoene *et al.*, 2008; Zeh *et al.*, 2009), which is documented by a number of larger TTG plutons in the Barberton Mountain Land (Table 4; Armstrong *et al.*, 1990; Zeh *et al.*, 2009). Various parts of the PB were accreted to the combined WB and SB between 3·1 and ~2·8 Ga (McCourt, 1995; Kröner *et al.*, 2000; Zeh *et al.*, 2009), whereas the KB was accreted to the eastern Kaapvaal at ~2·9 Ga (Schmitz *et al.*, 2004) and is therefore not relevant here.

Hence, during the inferred time of deposition of the ADT source sediments (<3175 Ma) and the intrusion of the granite itself (3067 Ma), the proto-Kaapvaal craton consisted only of the combined SB and WB (Fig. 8). The inherited zircon grains from the ADT granite will therefore be compared with samples from these two terranes in the Kaapvaal.

The oldest meta-volcanic rocks and TTG gneisses in the SB formed between ~3·64 and ~3·50 Ga (Fig. 9; Poujol *et al.*, 2003; Eglington & Armstrong, 2004; Kröner, 2007). Zircon grains from this age group were not discovered in the ADT granite in this study. The dominant group of TTG gneisses in the SB, however, formed from plutons intruded into the Barberton greenstone belt (BGB) between ~3·46 and 3·43 Ga (Poujol *et al.*, 2003). The 3433 ± 7 Ma age of the oldest ADT grains is indeed coeval with the ages of several TTG plutons in the Barberton region (Table 4). εHf_t values of zircons from those TTG are between −1·5 and +2·0 (Fig. 9; Amelin *et al.*, 2000; Zeh *et al.*, 2009, recalculated for the decay constant and CHUR composition used here). A number of Barberton TTG zircons are indistinguishable in Hf isotopes from the low-εHf_t group of the ADT granite (+1·5 ± 1·1).

Hf isotopic compositions close to the depleted mantle, as in the 3·43 Ga ADT high-εHf_t group, are as yet unknown for SB granitoid zircon. However, komatiite lavas in the BGB range from −0·4 to +7·1 (Blichert-Toft & Arndt, 1999; Blichert-Toft *et al.*, 2004, all recalculated) for a crystallization age of 3·45 Ga, and would therefore provide a

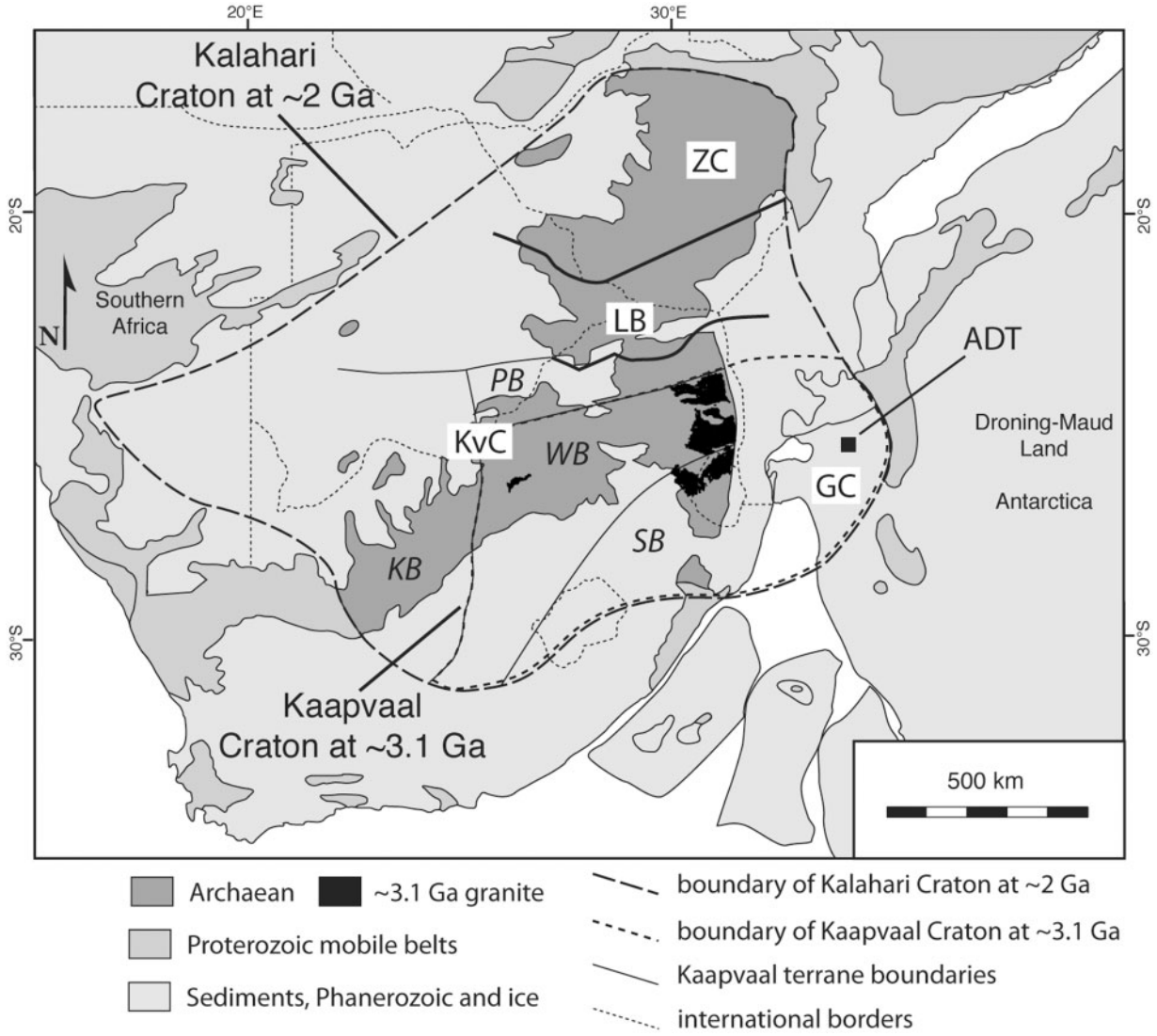

Fig. 8. Palaeogeographical juxtaposition of the Kalahari Craton (with present-day Africa coordinates), compiled from Hanson *et al.* (2004) and Jacobs *et al.* (2008*b*) with terrane structure and extent of ~3·1 Ga granite after Eglington & Armstrong (2004). ZC, Zimbabwe Craton; LB, Limpopo Belt; KvC, Kaapvaal Craton (consisting of the following terranes: PB, Pietersburg Block; KB, Kimberley Block; WB, Witwatersrand Block; SB, Swaziland Block). At 3·1 Ga, the Kaapvaal–Grunehogna Craton consisted of the SB, WB and GC as shown by the dashed line. It should be noted that in this widely accepted reconstruction the ADT granite exposures are located at a distance of only ~300 km from the Archaean of the SB and WB.

source for depleted-mantle-like Hf at the correct age (Fig. 9).

The ADT ~3·28 Ga age group has a corresponding range of trondjemitic rocks in the SB, namely in the Badplaas domain of the BGB (Kisters *et al.*, 2010). These relatively small plutons are interpreted as intrusions at the active continental margin of the SB between 3·29 and 3·23 Ga prior to its collision with the WB at ~3·23 Ga (Fig. 9; Kisters *et al.*, 2010). Hf isotope data for the Badplaas samples are not available, but based on a large set of samples Zeh *et al.* (2009) have shown that the Barberton TTG have εHf_t values close to CHUR at the relevant age, indistinguishable from the ADT 3·28 Ga grains ($\varepsilon Hf_t = -0{\cdot}2 \pm 1{\cdot}1$; Fig. 9; Table 4).

The collision between SB and WB at 3·23 Ga was accompanied by the intrusion of a larger number of tonalitic plutons in the AGC and BGB (e.g. Kamo & Davis, 1994; Poujol *et al.*, 2003; Schoene *et al.*, 2008). Zircon shows lower εHf_t values in the SB samples ($-1{\cdot}7 \pm 1{\cdot}1$) compared with the WB samples (up to +2·5; Zeh *et al.*, 2009), suggesting that the ADT inherited 3223 Ma grain ($\varepsilon Hf_t = -2{\cdot}8 \pm 1{\cdot}2$) is more closely related to the SB, and

Table 4: Comparison of zircon age and Hf data from the ADT (GC) with published data from the Kaapvaal Craton

Terrane:	Grunehogna Craton	Swaziland block	Witwatersrand block		Pietersburg block
Area:	ADT	Barberton S	Barberton N	Witwatersrand	Murchison + Giyani
	ADT	AGC			
Type	inherited	Stolzburg pluton			
Age (Ma)	3433 ± 7	3431 ± 11; 3440 ± 8			
εHf_t	+1·5 ± 1·1	+0·3 ± 1·6			
	+4·6 ± 0·6	−0·1 to + 2·0			
References		[2,4,5,16]			
		Theespruit			
Type		trondjemite pluton			
Age (Ma)		3437 ± 6; 3443 ± 3	No rock record, but detrital and inherited zircons		
εHf_t		+0·7 ± 0·6			
References		[2,3,6]			
		Hoggenoeg Fm			
Type		felsic flow			
Age (Ma)		3438 ± 6			
References		[1,2]			
	ADT	Badplaas domain			Giyani belt
Type	inherited	trondjemitic gneisses			tonalitic gneiss
Age (Ma)	3279 ± 9	e.g. 3282 ± 14*			3282·6 ± 0·4
εHf_t	−0·2 ± 1·1				
References		[15]			[11]
	ADT	Ngwane	Kaap Valley		MGB French Bob's Mine
Type	inherited	tonalitic gneiss	tonalite pluton		granite
Age (Ma)	3223 ± 8	3238 ± 8	3229 ± 5; 3227 ± 1		3228 ± 12
εHf_t	−2·8 ± 1·2	−1·7 ± 1·1	+2·5 ± 0·8		
References		[5]	[2,3,5,6,7]		[2,13]
			Stentor		
Type			granodiorite pluton		
Age (Ma)			3218 ± 9		
εHf_t			+0·9 ± 1·0		
References			[5,7]		
	ADT	AGC		Hartbeesfontein dome	Giyani belt
Type	inherited	leucogranite		peralum. granite	augengneiss
Age (Ma)	3175 ± 12	3166 ± 4		3174 ± 9	3170·5 ± 0·3
εHf_t	+1·1 ± 1·3				
References		[2,8]		[2,12]	[11]
	ADT	AGC, Pigg's peak	Cunningmore	Dominion gp	Makhutswi
Type	granite	potassic granite batholith	tonalite pluton	felsic rocks	tonalitic gneiss
Age (Ma)	3067 ± 8	3074 ± 4; 3099 ± 8	3049 ± 8	3074 ± 6	3063 ± 12
εHf_t	−0·5 ± 1·6	−0·1 ± 1·5	−0·6 ± 1·0		
References		[5]	[5]	[10]	[2,14]
		AGC, Sinceni	Salisbury	Vredefort Dome	
Type		peralum. granite pluton	granodiorite pluton	peralum. granite	
Age (Ma)		3074 ± 4	3105 ± 10	3101 ± 2	
εHf_t			−0·8 ± 1·1		
References		[2,6,9]	[2,5,6]	[2,12]	

[1] Kröner & Todt (1988), [2] Poujol *et al*. (2003), [3] Armstrong *et al*. (1990), [4] Dziggel *et al*. (2002), [5] Zeh *et al*. (2009), [6] Kamo & Davis (1994), [7] Tegtmeyer & Kröner (1987), [8] Kröner *et al*. (1989), [9] Trumbull (1993), [10] Armstrong *et al*. (1991), [11] Kröner *et al*. (2000), [12] Robb *et al*. (1992), [13] Poujol *et al*. (1996), [14] Poujol & Robb (1999), [15] Kisters *et al*. (2010), [16] Amelin *et al*. (2000). AGC, Ancient Gneiss Complex (Swaziland); ADT, Annandagstoppane (Antarctica); PGB, Pietersburg Greenstone Belt; MGB, Murchison Greenstone Belt.
*The trondjemitic gneisses of the Badplaas domain yield ages between 3·29 and 3·23 Ga. The age given here corresponds to one section of the domain (Kisters *et al*., 2010).

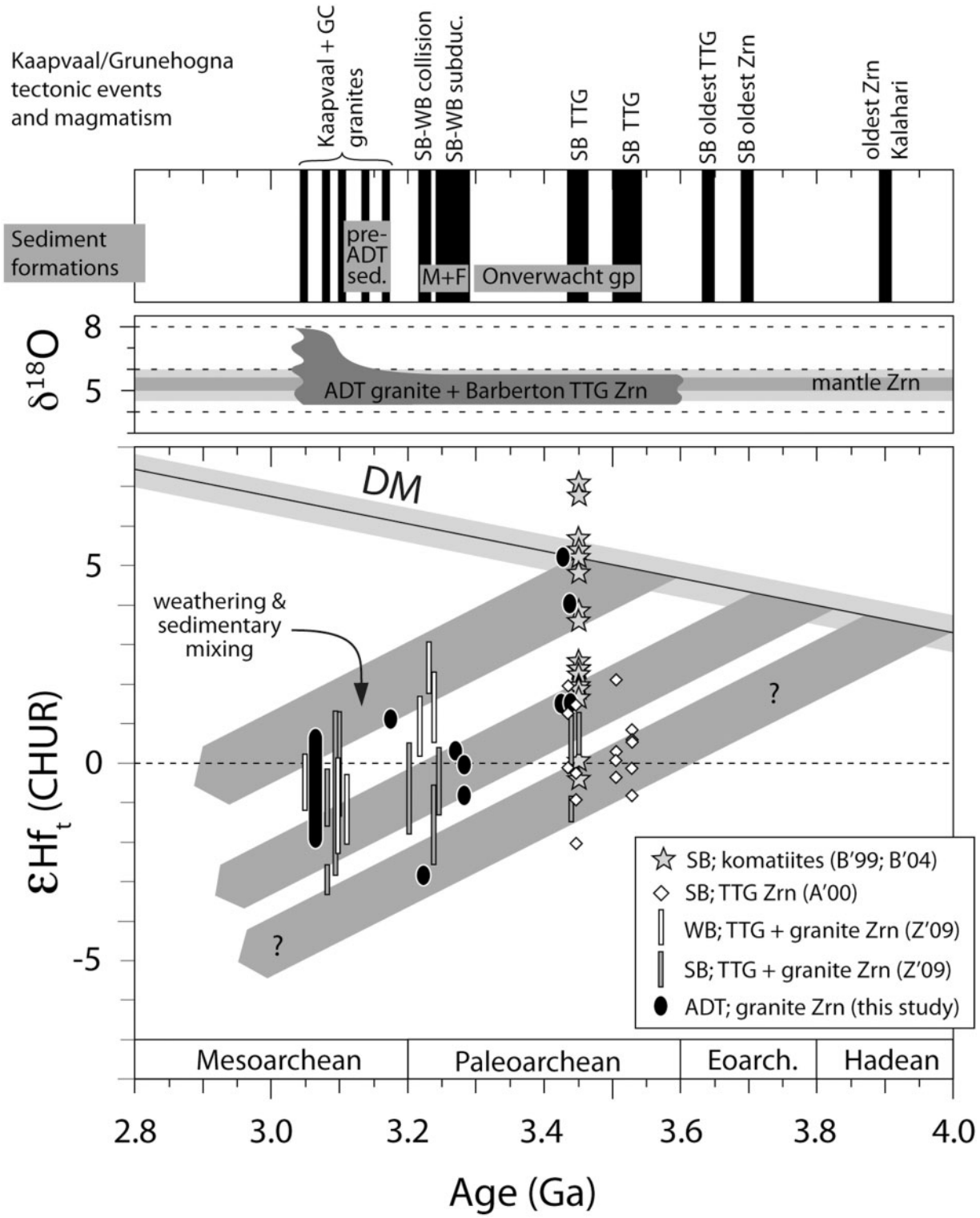

Fig. 9. Summary of geological events and geochronological and isotope data from the Kaapvaal and Grunehogna Cratons. Upper panel: age and duration of important tectonic events and magmatism indicated by width of black bars. 'pre-ADT sed.', proposed sedimentation age of the source sediments for the ADT granite; 'M+F', Moodies group and Fig Tree group. Data from Poujol *et al.* (2003), Kröner (2007), Zeh *et al.* (2008), Schoene *et al.* (2008) and van Kranendonk *et al.* (2009). Middle panel: O isotope evolution of zircon showing a significant increase at 3·1 Ga, as a result of significant reworking of supracrustal material during intracrustal differentiation. Lower panel: Hf isotopic evolution of SB, WB and GC zircon and SB komatiites. The two upper grey bars are identical to those in Fig. 7, whereas the lower one represents a group of SB sample with higher Hf model ages. This group includes only one grain from the ADT granite. Data sources: B'99, Blichert-Toft & Arndt (1999); B'04, Blichert-Toft *et al.* (2004); A'00, Amelin *et al.* (2000); Z'09, Zeh *et al.* (2009).

may represent crust with a higher Hf model age of ~3·90 Ga (Fig. 9). A larger group of 3·55–3·40 Ga and some 3·23 Ga Barberton TTG zircon grains also have lower εHf_t values and support a third trend in the Hf evolution diagram together with some komatiites and the 3·22 Ga inherited grain from the ADT granite (Fig. 9).

Some volumetrically minor granites intruded the SB and WB at ~3·17 Ga (Table 4), coeval with the ADT 3175 ± 12 Ma inherited grain, but no Hf isotope data are available for the former.

After the period of greenstone formation and TTG magmatism in the SB and WB, which lasted for ≥500 Myr, the continental crust of the combined terranes was intruded by a large potassic granite batholith at around 3·1 Ga, and by S-type leuco-granite plutons, such as the Sinceni pluton (Swaziland) at 3·07 Ga. This was accompanied by felsic volcanism, as, for example, in the Dominion Group of the Witwatersrand area (Table 4). The voluminous magmatism is thought to have assisted in stabilizing the crust and marks the onset of effective intracrustal differentiation in the Kaapvaal Craton (Schoene *et al.*, 2008; Zeh *et al.*, 2009). The crystallization age of the ADT granite post-dates the potassic granite batholiths in the eastern Kaapvaal Craton, but it is coeval with the smaller S-type plutons in the AGC, and with the felsic volcanic rocks in the Dominion Group (Table 4). Zircons from the SB and WB tonalites, granodiorites and potassic granites in this age group show uniform εHf_t values at *c.* −0·5 (Zeh *et al.*, 2009); that is, identical within error to those of the ADT granite (Fig. 9; Table 4).

Interestingly, the granite plutonism in the Kaapvaal Craton occurred within ~100 Myr between 3·14 and 3·04 Ga (Kamo & Davis, 1994; Schoene *et al.*, 2008) and indeed, the Archaean outcrop in the eastern Kaapvaal Craton today is vastly dominated by plutonic rocks emplaced within that time span (Eglington & Armstrong, 2004). Intrusion ages of ~3105 Ma strongly dominate this sequence (Kamo & Davis, 1994; Poujol *et al.*, 2003), but no inherited grains younger than 3175 Ma were found in the ADT granite.

The close similarity of the ages and Hf isotope composition of zircon from the SB (and WB) in the ADT zircon population suggests either that (1) the GC crust was identical in age and composition to the eastern Kaapvaal Craton in the Palaeo- and Mesoarchaean and simply formed an ~300 km eastern extension of the SB and WB (see Fig. 8), or that (2) the sediments that were the source of or intruded by the ADT granite were transported over that distance and deposited in the GC area. In the second case, the GC could be slightly younger than the eastern Kaapvaal, but must have also formed a continuous and stable continental unit with the eastern Kaapvaal Craton to allow for the transport, deposition and coeval reworking of the sediments across that distance.

The lack of any inherited zircon grains in the ADT granite of the 3105 Ma potassic granites vastly dominating the Archaean Kaapvaal suggests that the ADT granite source sediments were deposited prior to their emplacement and the associated felsic volcanism. This limits the deposition age of the ADT granite source sediments to the early Mesoarchaean between 3175 and 3105 Ma (Fig. 9).

Hf model ages and sedimentary mixing

Hf model ages for the ADT granite inherited zircons fall in two groups at $T_{DM} = 3{\cdot}50$ and 3·75 Ga, respectively, with minor evidence for even older crust. The number of near-concordant grains in the present study was limited and a larger sample set may or may not have led to a continuous range of model ages instead of the two discrete groups. However, that would not have changed the requirement for two or three crustal sources with different Hf isotopic compositions. Different sources are also apparent in the BGB, which essentially consists of komatiites and TTG gneisses. The 3·55–3·35 Ga TTG have εHf_t values partly corresponding to the high-T_{DM} group of ADT (3·75 Ga), and partly defining an older T_{DM} of ~3·90 Ga (Fig. 9).

The 3·45 Ga komatiites have εHf_t values spanning the full range between the $T_{DM} = 3{\cdot}50$ Ga and the 3·90 Ga groups with some values even plotting above the DM line. Hence, the different Hf model ages are indeed present in the SB, and the komatiites and TTG gneisses or related felsic volcanic rocks would form the most likely provenance for the Mesoarchaean sediment that is postulated as the source of the ADT granite. However, komatiite lavas do not contain reasonably sized zircon phenocrysts, hence the 3·43 Ga zircon grains with DM-like Hf isotopic compositions in the ADT granite point to a group of Palaeoarchaean TTG remelted from juvenile crust. Such granitoids have not yet been discovered in the Kaapvaal Craton, but they would place interesting constraints on the generation of felsic crust and tectonic processes in the early Archaean.

Humid weathering and erosion in the Mesoarchaean would have increased the $\delta^{18}O$ values of the deposited sediment, but it would not have influenced the mantle-like O isotopic composition of the detrital zircon grains. Supposedly the transport and deposition processes led to a sediment well mixed in Hf, with an εHf value intermediate between the two or three crustal sources.

The zircon crystallized from the granitic magma has elevated εHf values compared with the low-T_{DM} group of inherited grains. In various studies, such a 'rejuvenation' trend has been attributed to an addition of juvenile magma to the crust at the time of granite formation (e.g. Zeh *et al.*, 2009), with consequences for the geodynamic setting of the granites, for terrane boundaries and for the consolidation of the lithosphere. However, our example clearly demonstrates that the magma source was mixed

from two sources with crustal residence times of >350 Myr at the time of granite formation and that juvenile input over that entire period was insignificant.

Craton stabilization in the Mesoarchaean

Pre-3 Ga Archaean rock makes up a total outcrop area of ~26 000 km^2 in the combined SB and WB of the Kaapvaal Craton. Approximately 60% or ~15 000 km^2 of this is occupied by K-rich granite intrusions emplaced between 3·14 and 3·04 Ga (Fig. 8; area estimates from image analyses of maps from Eglington & Armstrong, 2004). Most of the outcrop is accessible on the eastern end of the Kaapvaal Craton, whereas large parts of the central and western sections are covered by younger sediments, volcanic rocks or younger intrusive rocks. However, in places where the craton can be sampled at domes or as xenoliths, the ~3·1 Ga high-K granite suite is also apparent in many places. This suggests that granites of this age range are not restricted to the eastern Kaapvaal, but may dominate the Archaean crust throughout the WB and SB and into the GC in the far east. Hence, they probably covered an area of ~250 000 km^2 and formed the most dominant component of the Kaapvaal middle to upper crust at 3·0 Ga.

Schoene *et al.* (2008) argued that widespread plutonism was a major mechanism in the mechanical stabilization of the Archaean crust. The granitic magmas transported heat-producing elements (K, U, Th) into higher crustal levels, leading to the establishment of cooler geothermal gradients in the lithosphere. In addition, the granite plutons and dykes crosscut all pre-existing crustal structures and, thereby, also enhanced the mechanical strength of the crust (Schoene *et al.*, 2008). The intrusion of the large granitic plutons is coeval with the last high-temperature (amphibolite- to granulite-facies) metamorphism in the Kaapvaal crust (Moser *et al.*, 2001). The Mesoarchaean at ~3 Ga is also thought to mark the final establishment of mechanical coupling of the crust to the underlying lithospheric mantle, and therefore the birth of the Kaapvaal 'tectosphere' (Moser *et al.*, 2001). After 3 Ga, the combined SB and WB formed the nucleus for the growing Kalahari Craton and did not undergo any further penetrative deformation or high-temperature metamorphism.

Crustal melting and widespread granitic plutonism clearly are major processes that operated in the crust during the establishment and stabilization of the craton. However, the cause of these intra-crustal differentiation processes in the Mesoarchaean (i.e. the cause for the rise of lower-crustal temperatures for ~100 Myr) is a matter of discussion. In general, a temperature increase in the crust may be achieved either by supplying heat from the underlying mantle or by lower crustal incubational heating. Enhanced heat transfer from the mantle is typically caused by thinning or delamination of the lithosphere and injection of significant amounts of mafic magmas into the crust. However, an increased mantle heat flux is incompatible with the establishment of the cool and buoyant subcontinental lithosphere in the Mesoarchaean Kaapvaal Craton, for which a decreasing heat flux to the crust during and after craton stabilization is predicted (Mareschal & Jaupart, 2006). This apparent paradox, with high-temperature metamorphism and anatexis in the crust overlying cooling lithospheric mantle, calls for intracrustal processes as causes for crustal melting (Mareschal & Jaupart, 2006).

Thermal crustal incubation without elevated heat flux from the mantle is caused by an increased crustal thickness or burial of rocks rich in heat-producing elements. Hence, widespread, relatively short-lived granitic plutonism caused by crustal incubation will produce granites with a very low or zero input of juvenile magma into the crust during granite genesis. In contrast, an input of juvenile magmas at 3·1 Ga would strongly support lithospheric thinning or delamination accompanied by mafic magmatism.

The zircon Hf isotope data from the Kaapvaal granites combined with the ADT granite demonstrate that juvenile contributions at 3·1 Ga were insignificant and the granites were generated from >350 Myr old crustal sources (Fig. 9). This provides evidence for incubational crustal heating as the cause for the massive Mesoarchaean intracrustal differentiation.

The zircon O isotope data show that the early Mesoarchaean (3·2–3·1 Ga) also marks the onset of deep burial of significant amounts of continental sediment. This provided a relatively felsic source for the K-rich granites, but, more importantly, it brought material highly enriched in heat-producing elements into deep crustal levels. Hence, the hypothesis established here is that the deep burial of continental sediments in the early Mesoarchaean caused a significant increase in the crustal geotherm, leading to anatexis and formation of widespread granitic plutonism for ~100 Myr. The granitic magmas returned the heat-producing elements to upper-crustal levels, relaxing the geothermal gradients, which led to the mechanical stabilization of the entire crust and the establishment of the Kaapvaal Craton.

This hypothesis derived from combined U–Pb dating and O–Hf isotope study of zircon is established in this study for the GC and the SB and WB blocks of the Kaapvaal Craton only. However, by investigating phenocrystic and xenocrystic zircon from Archaean granites in other terranes it will be possible to test whether intracrustal recycling of continental sediments is a major process of craton stabilization in all Archaean cratons or whether this was a unique feature of the Kaapvaal–Grunehogna Craton. A major advantage of the applied method is that it produces significant results with a minimum of preserved outcrop, as in the case of the GC, and is therefore

applicable even to very small or reworked portions of Archaean crust.

CONCLUSIONS

The Annadagstoppane granite in DML is the only outcrop of Archaean basement in the GC, which itself is the only Archaean fragment of West Gondwana in Antarctica. U–Pb dating of the youngest group of concordant zircons was employed to determine a crystallization age of 3067 ± 8 Ma. Inherited grains reflect tectono-magmatic events well known from the African Kaapvaal Craton. The GC formed the eastern extension of the Swaziland and Witwatersrand Blocks of the Kaapvaal Craton since at least 3105 Ma and possibly a part of the Swaziland Block as early as 3·50–3·75 Ga. The breakup of Gondwana, therefore, split a craton that was stable and intact for at least 2·5 billion years, until it was affected by continental-scale shear zones during the Panafrican orogeny (Jacobs & Thomas, 2004) and finally separated during the Jurassic (e.g. Martin & Hartnady, 1986).

Hafnium isotope compositions of phenocrystic and inherited zircons in the ADT granite show that the pluton contains a significant sedimentary component derived from at least two or three crustal sources with Hf model ages (T_{DM}) of ~3·50, ~3·75 and possibly ~3·90 Ga, respectively. The granite does not contain a significant juvenile component and, therefore, provides an example of pure intracrustal melting in the Mesoarchaean.

High-K granites intruded at 3·1 Ga form a major plutonic province in the Kaapvaal–Grunehogna Craton covering ~60% of the outcrop area. They played a major role in the mechanical stabilization of the continental crust during the establishment of the craton in the Mesoarchaean. Combined zircon Hf–O isotope data demonstrate that crustal melting and granite formation was caused by the deep burial of clastic sediments and subsequent incubational heating of the crust. It is suggested that intracrustal recycling of this type may be an important process in the long-term stabilization of continental crust.

ACKNOWLEDGEMENTS

Technical assistance during sample preparation by Alexander Weh (SelFrag) and by Eleanor Jennings (Bristol) is gratefully acknowledged. HRM greatly appreciates the support from Angela Helbling over the entire duration of this project. We thank J. Craven and R. Hinton (Ion Microprobe Facility, University of Edinburgh) for advice and guidance in obtaining the oxygen isotope and U–Pb data. Simon Harley, Joachim Jacobs and Stephen Daly are thanked for constructive reviews, and John Gamble is thanked for editorial handling. The British Antarctic Survey (BAS) is acknowledged for brilliant preparation for and organization of the field season and the logistics during the trip. Also, the Norwegian Polar Institute and the team of Troll station are thanked for actively supporting our field party.

FUNDING

This study was financially supported by the NERC Antarctic Funding Initiative (grant No. AFI7-03) and by a NERC analytical grant (grant No. IMF364/1008).

REFERENCES

Amelin, Y., Lee, D. C. & Halliday, A. N. (2000). Early–middle Archean crustal evolution deduced from Lu–Hf and U–Pb isotopic studies of single zircon grains. *Geochimica et Cosmochimica Acta* **64**, 4205–4225.

Armstrong, R. A., Compston, W., de Wit, M. J. & Williams, I. S. (1990). The stratigraphy of the 3·5–3·2 Ga Barberton greenstone belt revisited: a single zircon ion microprobe study. *Earth and Planetary Science Letters* **101**, 90–106.

Armstrong, R. A., Compston, W., Retief, E. A., Williams, I. S. & Welke, H. J. (1991). Zircon ion microprobe studies bearing on the age and evolution of the Witwatersrand triad. *Precambrian Research* **53**, 243–266.

Arndt, N. T., Todt, W., Chauvel, C., Tapfer, M. & Weber, K. (1991). U–Pb zircon age and Nd isotopic composition of granitoids, charnockites and supracrustal rocks from Heimefrontfjella, Antarctica. *Geologische Rundschau* **80**, 759–777.

Barton, J. M., Klemd, R., Allsopp, H. L., Auret, S. H. & Copperthwaite, Y. E. (1987). The geology and geochronology of the Annandagstoppane granite, Western Dronning Maud Land, Antarctica. *Contributions to Mineralogy and Petrology* **97**, 488–496.

Bisnath, A., Frimmel, H. E., Armstrong, R. A. & Board, W. S. (2006). Tectono-thermal evolution of the Maud Belt: new SHRIMP U–Pb zircon data from Gjelsvikfjella, Dronning Maud Land, Antarctica. *Precambrian Research* **150**, 95–121.

Black, L. P., Kamo, S. L., Allen, C. M., Davis, D. W., Aleinikoff, J. N., Valley, J. W., Mundil, R., Campbell, I. H., Korsch, R. J., Williams, I. S. & Foudoulis, C. (2004). Improved $^{206}Pb/^{238}U$ microprobe geochronology by the monitoring of a trace-element-related matrix effect: SHRIMP, ID-TIMS, ELA-ICP-MS and oxygen isotope documentation for a series of zircon standards. *Chemical Geology* **205**, 115–140.

Blichert-Toft, J. & Arndt, N. T. (1999). Hf isotope composition of komatiites. *Earth and Planetary Science Letters* **171**, 439–451.

Blichert-Toft, J., Arndt, N. T. & Gruau, G. (2004). Hf isotopic measurements on Barberton komatiites: effects of incomplete sample dissolution and importance for primary and secondary magmatic signatures. *Chemical Geology* **207**, 261–275.

Board, W. S., Frimmel, H. E. & Armstrong, R. A. (2005). Pan-African tectonism in the Western Maud Belt: *P–T–t* path for high-grade gneisses in H.U. Sverdrupfjella, East Antarctica. *Journal of Petrology* **46**, 671–699.

Boger, S. D. & Miller, J. M. (2004). Terminal suturing of Gondwana and the onset of the Ross–Delamerian orogeny: the cause and effect of an early Cambrian reconfiguration of plate motions. *Earth and Planetary Science Letters* **219**, 35–48.

Bouvier, A., Vervoort, J. D. & Patchett, J. P. (2008). The Lu–Hf and Sm–Nd isotopic composition of CHUR: constraints from

unequilibrated chondrites and implications for the bulk composition of terrestrial planets. *Earth and Planetary Science Letters* **273**, 48–57.

Collerson, K. D. & Kamber, B. S. (1999). Evolution of the continents and the atmosphere. *Science* **283**, 1519–1522.

Curtis, M. L. & Riley, T. R. (2003). Mobilization of fluidized sediment during sill emplacement, western Dronning Maud Land, East Antarctica. *Antarctic Science* **15**, 393–398.

de Wit, M. J., C, R., Hart, R. J., Armstrong, R. A., de Ronde, C. E. J., Green, R. W. E., Tredoux, M., Peberdy, E. & Hart, R. A. (1992). Formation of an Archean continent. *Nature* **357**, 553–562.

Dietz, R. S. & Sproll, W. P. (1970). Fit between Africa and Antarctica: a continental drift reconstruction. *Science* **167**, 1612–1614.

Dziggel, A., Stevens, G., Poujol, M., Anhaeusser, C. R. & Armstrong, R. A. (2002). Metamorphism of the granite–greenstone terrane south of the Barberton greenstone belt, South Africa: an insight into the tectono-thermal evolution of the 'lower' portions of the Onverwacht Group. *Precambrian Research* **114**, 221–247.

Eglington, B. M. & Armstrong, R. A. (2004). The Kaapvaal Craton and adjacent orogens, southern Africa: a geochronological database and overview of the geological development of the craton. *South African Journal of Geology* **107**, 13–32.

Fitzsimons, I. C. W. (2000). A review of tectonic events in the East Antarctic Shield and their implications for Gondwana and earlier supercontinents. *Journal of African Earth Sciences* **31**, 2–23.

Frimmel, H. E. (2004). Formation of a late Mesoproterozoic supercontinent: the South Africa–East Antarctica connection. In: Eriksson, P. G., Altermann, W., Nelson, D. R., Mueller, W. U. & Catuneanu, O. (eds) *The Precambrian Earth: Tempos and Events. Developments in Precambrian Geology* **12**, 240–255.

Golynsky, A. V. & Aleshkova, N. D. (2000). Regional magnetic anomalies of the Weddell Sea region and their geological significance. *Polarforschung* **67**, 101–107.

Grantham, G. H. (1996). Aspects of Jurassic magmatism and faulting in western Dronning Maud Land, Antarctica: implications for Gondwana break-up. In: Storey, B. C., King, E. C. & Livermore, R. A. (eds) *Weddell Sea Tectonics and Gondwana Break-up. Geological Society, London, Special Publications* **108**, 63–71.

Griffin, W. L., Wang, X., Jackson, S. E., Pearson, N. J., O'Reilly, S. Y., Xu, X. & Zhou, X. (2002). Zircon chemistry and magma mixing, SE China: *in situ* analysis of Hf isotopes, Tonglu and Pingtan igneous complexes. *Lithos* **61**, 237–269.

Groenewald, P. B., Grantham, G. H. & Watkeys, W. K. (1991). Geological evidence for a Proterozoic to Mesozoic link between southeastern Africa and Dronning Maud Land, Antarctica. *Journal of the Geological Society, London* **148**, 1115–1123.

Groenewald, P. B., Moyes, A. B., Grantham, G. H. & Krynauw, J. R. (1995). East Antarctic crustal evolution: geological constraints and modelling in western Dronning Maud Land. *Precambrian Research* **75**, 231–250.

Grosch, E. G., Bisnath, A., Frimmel, H. E. & Board, W. S. (2007). Geochemistry and tectonic setting of mafic rocks in western Dronning Maud Land, East Antarctica: implications for the geodynamic evolution of the Proterozoic Maud Belt. *Journal of the Geological Society, London* **164**, 465–475.

Halpern, M. (1970). Rubidium–strontium date of possibly 3 billion years for a granitic rock from Antarctica. *Science* **169**, 977–978.

Hanson, R. E., Crowley, J. L., Bowring, S. A., Ramezani, J., Gose, W. A., Dalziel, I. W. D., Pancake, J. A., Seidel, E. K., Blenkinsop, T. G. & Mukwakwami, J. (2004). Coeval large-scale magmatism in the Kalahari and Laurentian Cratons during Rodinia assembly. *Science* **304**, 1126–1129.

Hanson, R. E., Harmer, R. E., Blenkinsop, T. G., Bullen, D. S., Dalziel, I. W. D., Gose, W. A., Hall, R. P., Kampunzu, A. B., Key, R. M., Mukwakwami, J., Munyanyiwa, H., Pancake, J. A., Seidel, E. K. & Ward, S. E. (2006). Mesoproterozoic intraplate magmatism in the Kalahari Craton: a review. *Journal of African Earth Sciences* **46**, 141–167.

Hawkesworth, C. J. & Kemp, A. I. S. (2006). Using hafnium and oxygen isotopes in zircons to unravel the record of crustal evolution. *Chemical Geology* **226**, 144–162.

Ickert, R. B., Hiess, J., Williams, I. S., Holden, P., Ireland, T. R., Lanc, P., Schram, N., Foster, J. J. & Clement, S. W. (2008). Determining high precision, *in situ*, oxygen isotope ratios with a SHRIMP II: analyses of MPI-DING silicate-glass reference materials and zircon from contrasting granites. *Chemical Geology* **257**, 114–128.

Jacobs, J. & Thomas, R. J. (2004). Himalayan-type indenter-escape tectonics model for the southern part of the late Neoproterozoic–early Paleozoic East African–Antarctic orogen. *Geology* **32**, 721–724.

Jacobs, J., Fanning, C. M., Henjes-Kunst, F., Olesch, M. & Paech, H. J. (1998). Continuation of the Mozambique Belt into East Antarctica: Grenville-age metamorphism and polyphase Pan-African high-grade events in Central Dronning Maud Land. *Journal of Geology* **106**, 385–406.

Jacobs, J., Bauer, W. & Fanning, C. M. (2003*a*). New age constraints for Grenville-age metamorphism in western central Dronning Maud Land (East Antarctica), and implications for the palaeogeography of Kalahari in Rodinia. *International Journal of Earth Sciences* **92**, 301–315.

Jacobs, J., Bauer, W. & Fanning, C. M. (2003*b*). Late Neoproterozoic/Early Palaeoproterozoic events in central Dronning Maud Land and significance for the southern extension of the East African Orogen into East Antarctica. *Precambrian Research* **126**, 27–53.

Jacobs, J., Bingen, B., Thomas, R. J., Bauer, W., Wingate, M. T. D. & Feitio, P. (2008*a*). Early Palaeozoic orogenic collapse and voluminous late-tectonic magmatism in Dronning Maud Land and Mozambique: insights into the partially delaminated orogenic root of the East African–Antarctic Orogen? In: Satish-Kumar, M., Motoyoshi, Y., Osanai, Y., Hiroi, Y. & Shiraishi, K. (eds) *Geodynamic Evolution of East Antarctica: a Key to the East–West Gondwana Connection Geological Society, London, Special Publications* **308**, 69–90.

Jacobs, J., Pisarevsky, S., Thomas, R. J. & Becker, T. (2008*b*). The Kalahari Craton during the assembly and dispersal of Rodinia. *Precambrian Research* **160**, 142–158.

Jones, D. L., Bates, M. P., Li, Z. X., Corner, B. & Hodgkinson, G. (2003). Palaeomagnetic results from the ca. 1130 Ma Borgmassivet intrusions in the Ahlmannryggen region of Dronning Maud Land, Antarctica, and tectonic implications. *Tectonophysics* **375**, 247–260.

Kamo, S. L. & Davis, D. W. (1994). Reassessment of Archean crustal development in the Barberton Mountain Land, South Africa, based on U–Pb dating. *Tectonics* **13**, 167–192.

Kelly, N. M., Hinton, R. W., Harley, S. L. & Appleby, S. (2008). New SIMS U–Pb zircon ages from the Langavat Belt, South Harris, NW Scotland: implications for the Lewisian Terrane model. *Journal of the Geological Society, London* **165**, 967–981.

Kemp, A. I. S., Hawkesworth, C. J., Paterson, B. A. & Kinny, P. D. (2006). Episodic growth of the Gondwana supercontinent from hafnium and oxygen isotopes in zircon. *Nature* **439**, 580–583.

Kemp, A. I. S., Hawkesworth, C. J., Foster, G. L., Paterson, B. A., Woodhead, J. D., Hergt, J. M., Gray, C. M. & Whitehouse, M. J. (2007). Magmatic and crustal differentiation history of granitic rocks from Hf–O isotopes in zircon. *Science* **315**, 980–983.

Kisters, A. F. M., Belcher, R. W., Poujol, M. & Dziggel, A. (2010). Continental growth and convergence-related arc plutonism in the Mesoarchaean: evidence from the Barberton granitoid–greenstone terrain, South Africa. *Precambrian Research* (in press), doi:10.1016/j.precamres.2010.01.002.

Kröner, A. (2007). The Ancient Gneiss Complex of Swaziland and environs: record of early Archean crustal evolution in southern Africa. In: van Kranendonk, M. J., Smithies, R. H. & Bennett, V. C. (eds) *Earth's Oldest Rocks. Developments in Precambrian Geology* **15**, 465–480.

Kröner, A. & Todt, W. (1988). Single zircon dating containing the maximum age of the Barberton greenstone belt, southern Africa. *Journal of Geophysical Research* **93**, 15329–15337.

Kröner, A., Compston, W. & Williams, I. S. (1989). Growth of early Archean crust in the Ancient Gneiss Complex of Swaziland as revealed by single zircon dating. *Tectonophysics* **161**, 271–298.

Kröner, A., Jaeckel, P. & Brandl, G. (2000). Single zircon ages for felsic to intermediate rocks from the Pietersburg and Giyani greenstone belts and bordering granitoid orthogneisses, northern Kaapvaal Craton, South Africa. *Journal of African Earth Sciences* **30**, 773–793.

Krynauw, J. R., Hunter, D. R. & Wilson, A. H. (1988). Emplacement of sills into wet sediments at Grunehogna, western Dronning Maud Land, Antarctica. *Journal of the Geological Society, London* **145**, 1019–1032.

Leat, P. T., Dean, A. A., Millar, I. L., Kelley, S. P., Vaughan, A. P. M. & Riley, T. R. (2005). Lithospheric mantle domains beneath Antarctica. In: Vaughan, A. P. M., Leat, P. T. & Pankhurst, R. J. (eds) *Terrane Processes at the Margins of Gondwana. Geological Society, London, Special Publications* **246**, 359–380.

Ludwig, K. R. (2003). *User's manual for Isoplot 3.00—a geochronological toolkit for Microsoft Excel. Berkeley Geochronology Center Special Publications* **4**.

Luttinen, A. V. & Furnes, H. (2000). Flood basalts of Vestfjella: Jurassic magmatism across an Archean–Proterozoic lithospheric boundary in Dronning Maud Land, Antarctica. *Journal of Petrology* **41**, 1271–1305.

Mareschal, J. C. & Jaupart, C. (2006). Archean thermal regime and stabilization of the cratons. In: Benn, K., Mareschal, J. C. & Condie, K. C. (eds) *Archean Geodynamics and Environments. Geophysical Monograph, American Geophysical Union* **164**, 61–73.

Martin, A. K. & Hartnady, C. J. H. (1986). Plate tectonic development of the South West Indian Ocean: a revised reconstruction of East Antarctica and Africa. *Journal of Geophysical Research* **19**, 4767–4786.

McCourt, S. (1995). The crustal architecture of the Kaapvaal crustal block South Africa, between 3·5 and 2·0 Ga. *Mineralium Deposita* **30**, 89–97.

Moser, D. E., Flowers, R. M. & Hart, R. J. (2001). Birth of the Kaapvaal tectosphere 3·08 billion years ago. *Science* **291**, 465–468.

Moyes, A. B., Barton, J. M. & Groenewald, P. B. (1993). Late Proterozoic to Early Palaeozoic tectonism in Dronning Maud Land, Antarctica: supercontinental fragmentation and amalgamation. *Journal of the Geological Society, London* **150**, 833–842.

Peck, W. H., Valley, J. W., Wilde, S. A. & Graham, C. M. (2001). Oxygen isotope ratios and rare earth elements in 3·3 to 4·4 Ga zircons: ion microprobe evidence for high $\delta^{18}O$ continental crust and oceans in the Early Archean. *Geochimica et Cosmochimica Acta* **65**, 4215–4229.

Pietranik, A. B., Hawkesworth, C. J., Storey, C. D., Kemp, A. I. S., Sircombe, K. N., Whitehouse, M. J. & Bleeker, W. (2008). Episodic, mafic crust formation from 4·5 to 2·8 Ga: new evidence from detrital zircons, Slave craton, Canada. *Geology* **36**, 875–878.

Poujol, M. & Robb, L. J. (1999). New U–Pb zircon ages on gneisses and pegmatite from south of the Murchison greenstone belt, South Africa. *South African Journal of Geology* **102**, 93–97.

Poujol, M., Robb, L. J., Respaut, J. P. & Anhaeusser, C. R. (1996). 3·07–2·97 Ga greenstone belt formation in the northeastern Kaapvaal Craton: implications for the origin of the Witwatersrand Basin. *Economic Geology* **91**, 1455–1461.

Poujol, M., Robb, L. J., Anhaeusser, C. R. & Gericke, B. (2003). A review of the geochronological constraints on the evolution of the Kaapvaal Craton, South Africa. *Precambrian Research* **127**, 181–213.

Powell, C. M., Jones, D. L., Pisarevsky, S. & Wingate, M. T. D. (2001). Palaeomagnetic constraints on the position of the Kalahari craton in Rodinia. *Precambrian Research* **110**, 33–46.

Robb, L. J., Davis, D. W., Kamo, S. L. & Meyer, F. M. (1992). Ages of altered granites adjoining the Witwatersrand Basin with implications for the origin of gold and uranium. *Nature* **357**, 677–680.

Scherer, E. E., Münker, C. & Mezger, K. (2001). Calibration of the lutetium–hafnium clock. *Science* **293**, 683–687.

Schmitz, M. D., Bowring, S. A., de Wit, M. J. & Gartz, V. (2004). Subduction and terrane collision stabilized the western Kaapvaal craton tectosphere 2·9 billion years ago. *Earth and Planetary Science Letters* **222**, 363–376.

Schoene, B., de Wit, M. J. & Bowring, S. A. (2008). Mesoarchean assembly and stabilization of the eastern Kaapvaal craton: a structural–thermochronological perspective. *Tectonics* **27**, TC5010, doi:10.1029/2008TC002 267.

Schuhmacher, M., de Chambost, E., McKeegan, K. D., Harrison, T. M. & Midgeon, H. (1994). *In-situ* dating of zircon with the Cameca ims-1270. In: Benninghoven, A., Nihel, Y., Shimizu, R. & Werner, H. W. (eds) *Secondary Ion Mass Spectrometry.* New York: Wiley, pp. 919–922.

Smith, A. G. & Hallam, A. (1970). The fit of the southern continents. *Nature* **225**, 139–144.

Söderlund, U., Patchett, J. P., Vervoort, J. D. & Isachsen, C. E. (2004). The ^{176}Lu decay constant determined by Lu–Hf and U–Pb isotope systematics of Precambrian mafic intrusions. *Earth and Planetary Science Letters* **219**, 311–324.

Taylor, S. R. & McLennan, S. M. (2009). *Planetary Crusts—their Composition, Origin and Evolution.* Cambridge: Cambridge University Press.

Tegtmeyer, A. R. & Kröner, A. (1987). U–Pb zircon ages bearing on the nature of early Archean greenstone belt evolution, Barberton Mountain Land, southern Africa. *Precambrian Research* **36**, 1–20.

Trumbull, R. B. (1993). A petrological and Rb–Sr isotopic study of an early Archean fertile granite-pegmatite system: the Sinceni Pluton in Swaziland. *Precambrian Research* **61**, 89–116.

Valley, J. W. (2003). Oxygen isotopes in zircon. In: Hanchar, J. M. & Hoskin, P. W. O. (eds) *Zircon. Mineralogical Society of America and Geochemical Society, Reviews in Mineralogy and Geochemistry* **53**, 343–385.

Valley, J. W., Lackey, J. S., Cavosie, A. J., Clechenko, C. C., Spicuzza, M. J., Basei, M. A. S., Bindemann, I. N., Ferreira, V. P., Sial, A. N., King, E. M., Peck, W. H., Sinha, A. K. & Wei, C. S. (2005). 4·4 billion years of crustal maturation: oxygen isotope ratios of magmatic zircon. *Contributions to Mineralogy and Petrology* **150**, 561–580.

van Kranendonk, M. J., Kröner, A., Hegner, E. & Connelly, J. (2009). Age, lithology and structural evolution of the c. 3·53 Ga Theespruit Formation in the Tjakastad area, southwestern Barberton Greenstone Belt, South Africa, with implications for Archaean tectonics. *Chemical Geology* **261**, 115–139.

van Reenen, D. D., Barton, J. M., C, R., Smit, C. A. & van Schalkwyk, J. F. (1987). Deep crustal response to continental collision: the Limpopo belt of southern Africa. *Geology* **15**, 11–14.

Wareham, C. D., Pankhurst, R. J., Thomas, R. J., Storey, B. C., Grantham, G. H., Jacobs, J. & Eglington, B. M. (1998). Pb, Nd, and Sr isotope mapping of Grenville-age crustal provinces in Rodinia. *Journal of Geology* **106**, 647–659.

Wiedenbeck, M., Alle, P., Corfu, F., Griffin, W. L., Meier, M., Oberli, F., von Quadt, A., Roddick, J. C. & Spiegel, W. (1995). 3 natural zircon standards for U–Th–Pb, Lu–Hf, trace-element and REE analyses. *Geostandards Newsletter* **19**, 1–23.

Wiedenbeck, M., Hanchar, J. M., Peck, W. H., Sylvester, P., Whitehouse, M. J., Kronz, A., Morishita, Y., Nasdala, L., Fiebig, J., Franchi, I., Girard, J. P., Greenwood, R. C., Hinton, R. W., Kita, N., Mason, P. R. D., Norman, M., Ogasawara, M., Piccoli, P. M., Rhede, D., Satoh, H., Schulz-Dobrick, B., Skår, O., Spicuzza, M. J., Terada, K., Tindle, A., Togashi, S., Vennemann, T., Xie, Q. & Zheng, Y. F. (2004). Further characterisation of the 91500 zircon crystal. *Geostandards and Geoanalytical Research* **28**, 9–39.

Wilde, S. A., Valley, J. W., Peck, W. H. & Graham, C. M. (2001). Evidence from detrital zircons for the existence of continental crust and oceans on the Earth 4·4 Gyr ago. *Nature* **409**, 175–178.

Wolmarans, L. G. & Kent, L. E. (1982). Geological investigations in western Dronning Maud Land, Antarctica—a synthesis. *South African Journal of Antarctic Research* **2**, 1–93.

Zeh, A., Gerdes, A., Klemd, R. & Barton, J. M. (2008). U–Pb and Lu–Hf isotope record of detrital zircon grains from the Limpopo Belt—Evidence for crustal recycling at the Hadean to early-Archean transition. *Geochimica et Cosmochimica Acta* **72**, 5304–5329.

Zeh, A., Gerdes, A. & Barton, J. M. (2009). Archaean accretion and crustal evolution of the Kalahari Craton—the zircon age and Hf Isotope record of granitic rocks from Barberton/Swaziland to the Francistown arc. *Journal of Petrology* **50**, 933–966.